Planetary-Scale Shear Trajectories and Their Expression in Global Geological Geometry

Craig Stone

16 December 2025

Plain Language Summary

Earth's surface contains enormous curved features: sweeping sediment belts, arcing mountain chains, curved chains of lakes, broad bends in the ocean floor, and large tectonic arcs. These features are typically explained individually using local processes such as erosion, sediment transport, glaciation, or plate collision.

This study shows that many of these features align with a single global pattern of surface stress. When a mathematically derived shear field—expected during large, rapid reorientation of Earth's rotation axis—is overlaid on modern maps, it aligns with geological features across continents and oceans.

The alignment appears in loose sediments, rigid continental crust, active mountain belts, rift systems, glacial landscapes, and even mid-ocean ridges that are continuously forming today. This consistency suggests that Earth's surface geometry may be influenced by a long-wavelength, planet-scale stress framework operating alongside plate tectonics, rather than being determined solely by local processes.

Abstract

Large arcuate geological features occur across Earth's surface in sedimentary, tectonic, and oceanic environments. While individual examples are commonly attributed to local processes, their global geometric coherence has received limited systematic examination.

We compare global geological and geophysical datasets with analytically derived surface shear trajectories associated with a prescribed class of true polar wander (TPW) geometries. Using a Vening Meinesz–style formulation, two conjugate shear families (Net 1 and Net 2) and invariant contours are computed analytically on the sphere and projected without tuning to geological data.

Systematic geometric congruence is documented between the modeled shear field and a wide range of features, including continental sediment arcs, major mountain belts, oceanic bathymetric curvature, rift systems, glacially sculpted terrains, and actively forming plate boundaries. A quantitative comparison with the World Stress Map (WSM) database shows that, while the

global aggregate misfit is not statistically distinguishable from random expectation, strong and spatially coherent regional agreement is observed across multiple tectonic settings.

The recurrence of these alignments across lithospheric ages, tectonic regimes, and material behaviors suggests that Earth's surface geometry may be influenced by a long-wavelength, planet-scale stress topology compatible with whole-Earth reorientation acting as a persistent organizing framework operating alongside plate tectonics, rather than being determined solely by local processes.

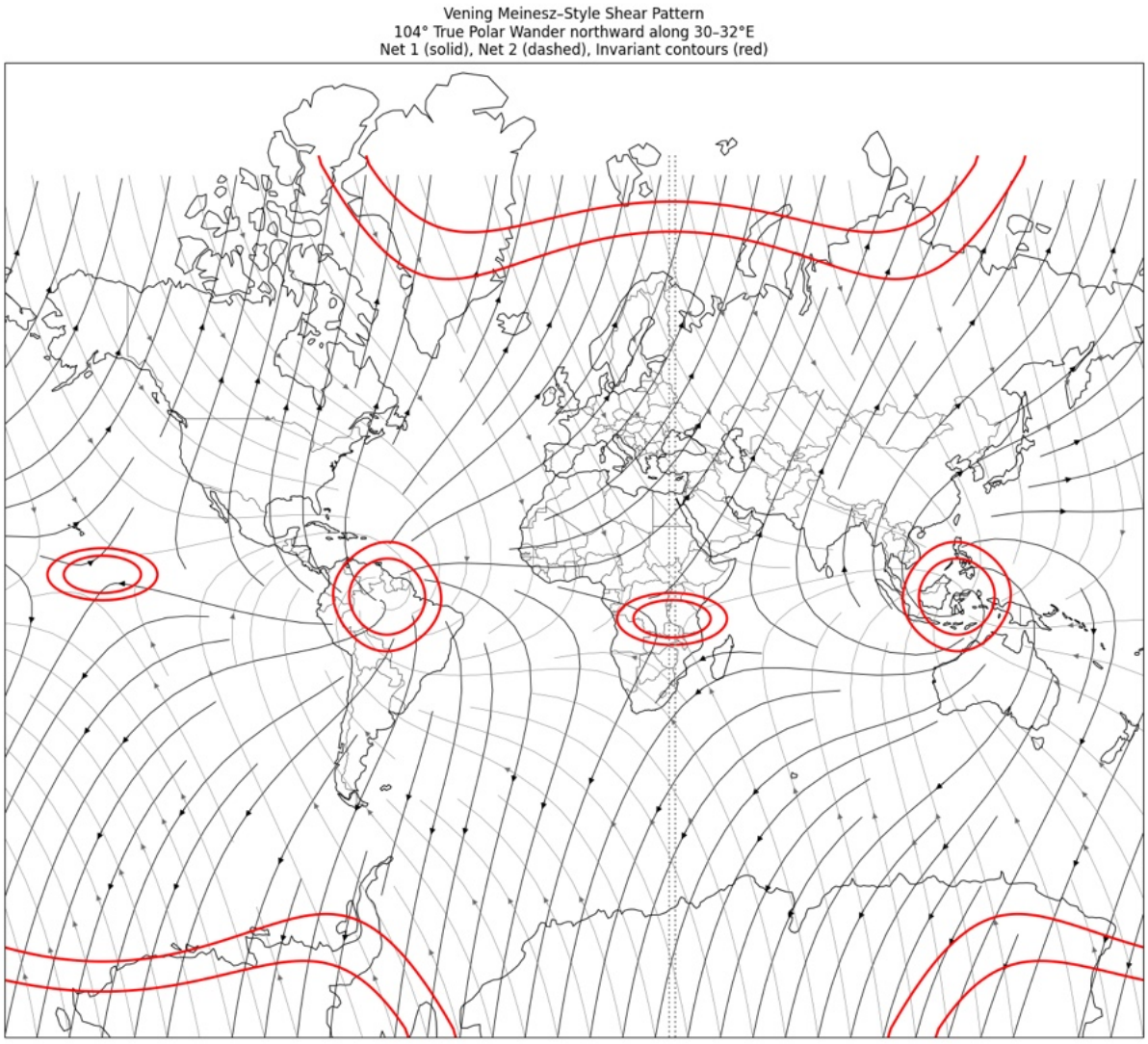

Figure 1: Vening Meinesz–style global shear pattern for a prescribed 104° northward true polar wander along the 31°E meridian. Solid curves indicate Net 1 shear trajectories, dashed curves Net 2 trajectories, and red curves invariant contours.

1 Introduction

Earth's lithosphere exhibits pervasive curvature at continental and planetary scales. Arcuate sediment belts, sweeping mountain chains, curved continental margins, bathymetric arcs, rift systems, and coherent chains of basins occur across disparate tectonic environments and geological ages.

Conventional explanations typically invoke local boundary conditions—such as plate convergence, inherited basement fabric, mantle flow, glaciation, or sediment routing—to explain individual cases [Turcotte and Schubert, 2014, Condie, 1997]. However, many of the largest arcs cross geological provinces, persist across lithospheric ages, and display smooth, continuous curvature that is difficult to reconcile with segmented tectonic histories or short-wavelength forcing alone.

These observations motivate examination of whether Earth's surface geometry reflects a deeper, planet-scale stress framework associated with whole-Earth dynamics such as true polar wander.

2 Methods

2.1 Prescribed True Polar Wander Geometry

A single TPW scenario is specified as a rigid-body northward rotation of 104° about an axis fixed along the 31°E meridian. The transformation is treated geometrically, without assumptions regarding timing, rate, or physical driver. The purpose is not to reconstruct a specific event, but to evaluate whether such a geometry produces a stress topology consistent with observed geological structure.

2.2 Construction of the Global Shear Field

The surface stress field is represented by two orthogonal families of shear trajectories:

- **Net 1**: trajectories aligned with maximum differential shear induced by reorientation.
- **Net 2**: trajectories orthogonal to Net 1, representing conjugate shear accommodation.

Invariant contours are computed as loci of minimal differential shear. All trajectories are generated analytically on the sphere and projected without fitting to geological data.

2.3 Datasets and Visualization

Independent datasets include global plate boundaries, bathymetry, geological provinces, surface sediment composition, digital elevation models, satellite imagery, and the World Stress Map (WSM) 2025 database. Multiple map projections, including polar stereographic views, are used to reduce projection bias and test robustness.

3 Results: Regional Case Studies

3.1 Southeastern United States Sediment Arc

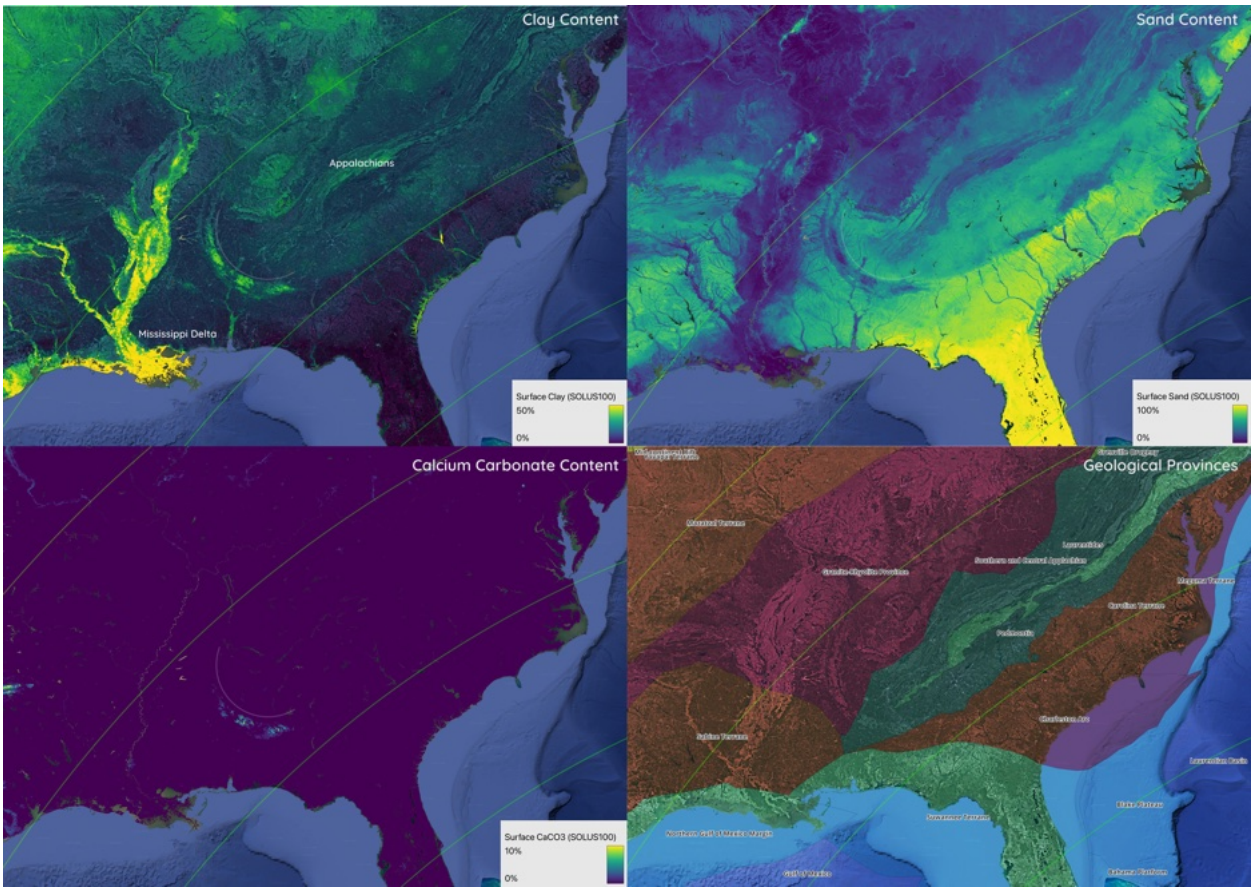

Figure 2: Four-panel comparison of clay, $CaCO_3$, sand, and geological provinces in the southeastern United States. A continent-scale arcuate belt aligns with invariant shear contours and crosses multiple geological provinces.

The arcuate sedimentary belt spanning the southeastern United States (Figure 2) represents one of the clearest expressions of the modeled global shear framework acting within a passive-margin setting. This feature is conventionally explained through a combination of Appalachian orogenic inheritance, differential erosion, fluvial routing, and marine sediment redistribution. While these processes are undoubtedly active contributors, they do not readily account for the remarkable geometric coherence, continuity, and scale of the arc across multiple sediment classes and geological provinces.

When examined in the context of the global shear model, the sediment arc aligns closely with invariant shear contours, rather than with present-day drainage basins, coastline geometry, or individual tectonostratigraphic boundaries. The arc persists across terranes of differing lithology and age, including Paleozoic orogenic belts, Mesozoic rifted margins, and Cenozoic sedimentary

platforms. This independence from local structural segmentation strongly suggests that the arc reflects a preconditioning stress geometry rather than a product of basin-scale processes alone.

Notably, the congruence is observed simultaneously in clay-rich sediments, carbonate distributions, and sandy deposits, each of which responds differently to transport mechanisms, chemical weathering, and depositional environments. The convergence of these distinct sedimentary signals along the same arcuate trajectory argues against coincidental alignment and instead points to a shared controlling framework. Within the shear-net interpretation, this framework corresponds to zones of minimal differential shear, which would preferentially localize long-term sediment accumulation by suppressing disruptive deformation while subtly biasing transport pathways.

The southeastern sediment arc thus appears to function as a geomorphic and sedimentological amplifier of an inherited lithospheric stress architecture. Over geological time, repeated episodes of erosion, sea-level change, and sediment reworking have progressively revealed and reinforced this geometry rather than obscuring it. This behavior mirrors that observed in other regions of the study, where weak or ductile surface materials act as high-fidelity recorders of low-order, long-wavelength stress fields.

Importantly, this reinterpretation does not negate established Appalachian or passive-margin models. Instead, it reframes them within a hierarchical context: local tectonics and surface processes operate within, and are subtly guided by, a persistent planetary-scale shear topology. In this view, the southeastern United States sediment arc represents not an isolated geomorphic curiosity, but a continental-scale manifestation of the same stress framework expressed in mountain belts, rift systems, and oceanic structures elsewhere on Earth.

3.2 The Himalayan Arc

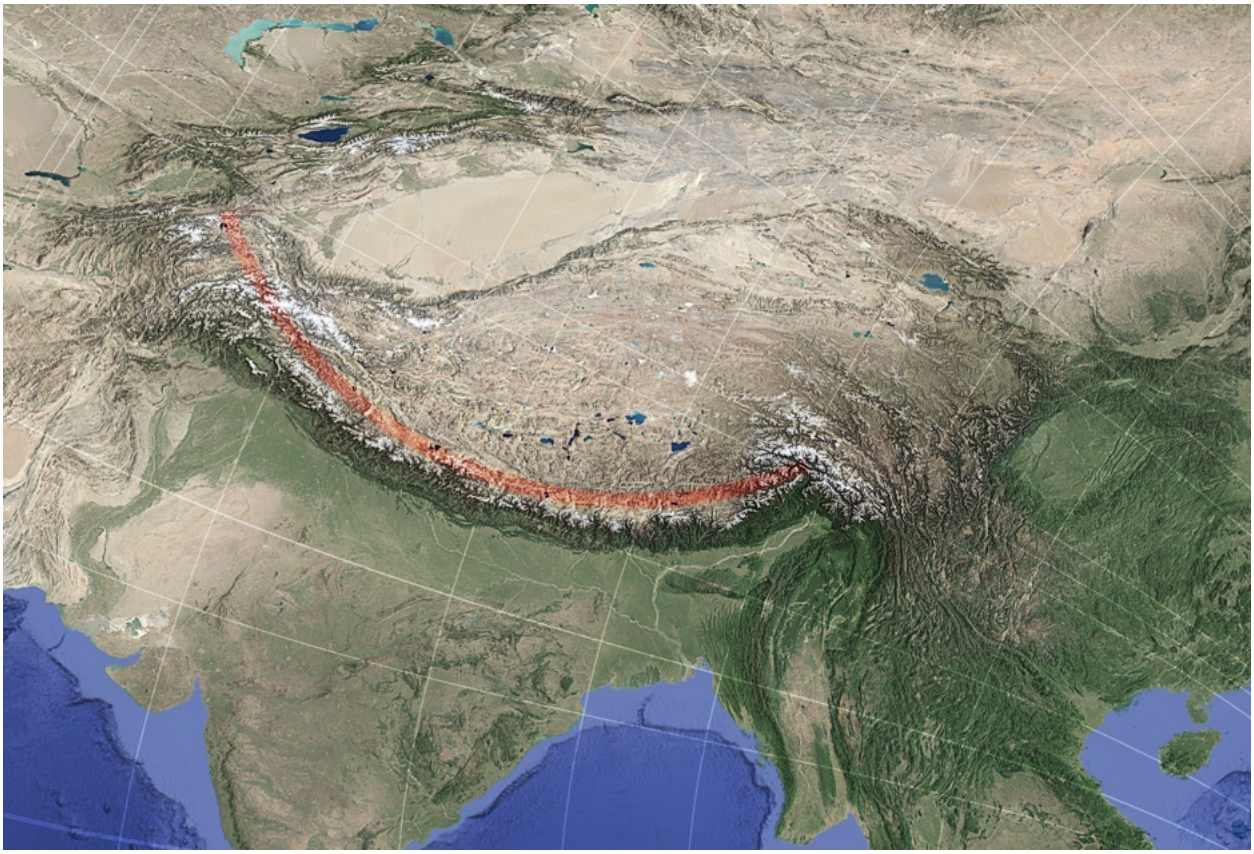

Figure 3: The Himalayan mountain belt forms a geometrically smooth arc that lies parallel to one shear family and orthogonal to the conjugate family.

The Himalayan orogen constitutes one of the most striking large-scale arcuate features on Earth, traditionally interpreted as the product of continent–continent collision between the Indian and Eurasian plates. While this tectonic framework successfully explains crustal shortening, uplift, and seismicity, it does not by itself account for the exceptional geometric regularity of the Himalayan arc over more than 2,500 km, nor for its consistent orientation relative to global stress fields.

Within the global shear-net model, the Himalayan arc exhibits a near-ideal orthogonality to one family of shear trajectories (Net 1) while remaining approximately parallel to the complementary set (Net 2). This dual relationship is non-trivial: it implies that the arc occupies a geometric locus where principal shear directions transition from compressional to tangential dominance. In such a configuration, convergent deformation would be expected to organize into a smooth, laterally continuous curvature rather than fragmenting into irregular salients or segmented thrust systems.

The persistence of this geometry across regions of highly variable crustal thickness, lithology, and tectonic inheritance suggests that the Himalayan arc is not solely a local collision artifact, but instead a lithospheric-scale response to a pre-existing stress topology. In this interpretation,

the India–Asia collision acts as an energy source that activates and amplifies a globally imposed shear pattern, rather than generating the observed curvature independently. The arc is thus a mechanically optimal configuration for accommodating shortening within a broader, planet-scale stress field.

This perspective helps reconcile several long-standing anomalies in Himalayan geology. The relative uniformity of arc curvature contrasts with the heterogeneity of convergence rates, slab geometries, and plateau uplift across the orogen. Additionally, the lateral continuity of major thrust systems and the coherence of foreland basin development align more naturally with a guiding stress geometry than with purely local structural inheritance. The shear-net framework provides such a guide, offering a geometric constraint that operates above the scale of individual faults or terranes.

Furthermore, the Himalayan arc finds analogues in other arcuate systems identified in this study, including the Andes, the Banda Arc, the Caribbean, and selected intracontinental features. In each case, large-scale curvature coincides with regions where the modeled shear trajectories impose a stable, low-variance stress configuration. The Himalaya thus represents an end-member example of how extreme tectonic forcing can be geometrically channeled by a persistent global stress architecture.

In summary, the Himalayan arc is best understood not as a purely emergent property of continental collision, but as the visible outcome of collision occurring within a pre-organized, long-wavelength shear field. This reinterpretation preserves the successes of plate tectonic theory while extending it to incorporate a higher-order, global geometrical control that appears repeatedly throughout the geological record.

3.3 Central America and the Caribbean

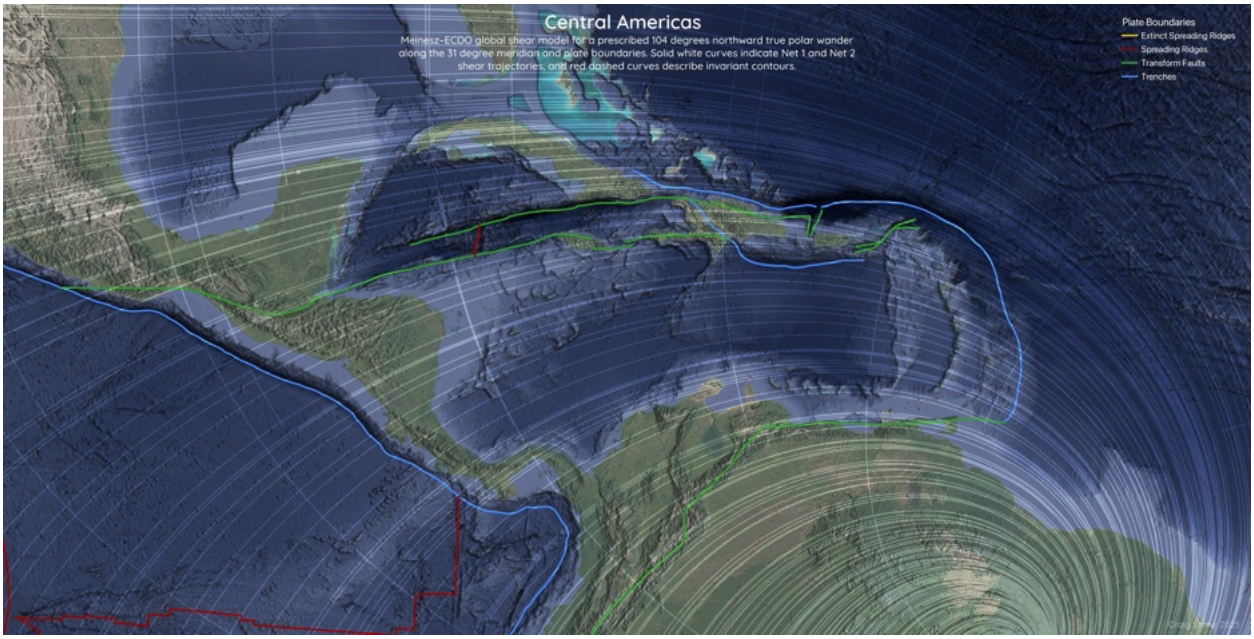

Figure 4: Central America and the Caribbean showing strong geometric congruence between plate boundaries and the modeled global shear field.

3.4 Central America and the Caribbean: Shear-Guided Arc Segmentation and Plate-Boundary Organization

Central America and the Caribbean constitute one of the most tectonically intricate regions on Earth, involving interactions among multiple major and minor plates, variable subduction polarity, transform faulting, microplate rotation, and inherited continental fragments. Conventional plate-kinematic models successfully describe relative motions within this system, but they do not fully account for the pronounced geometric coherence, curvature continuity, and segmentation observed across arcs, basins, and fault systems at regional to supra-regional scales.

When examined within the global shear-net framework, Central America and the Caribbean occupy a region of pronounced shear curvature and net convergence associated with the western Euler-point domain. The dominant arcs of the Lesser Antilles, Central American volcanic front, and the curved margins of the Caribbean Plate closely parallel modeled shear trajectories rather than strictly following instantaneous plate motion vectors. This alignment persists across transitions from oceanic to continental lithosphere and across boundaries separating subduction-dominated, transform-dominated, and extensional regimes.

A particularly diagnostic feature is the smooth curvature of the Caribbean Plate margins. Rather than forming a simple polygonal plate outline, the plate boundary traces long-radius arcs that correspond closely to invariant shear contours. These contours represent loci of minimal differential shear, where long-term structural persistence would be expected. The resulting geometry

provides a natural explanation for the stability of the Caribbean Plate as a coherent entity despite its complex internal deformation and prolonged tectonic isolation.

Rift boundaries and major transform systems within the region exhibit mixed but non-random behavior. Several major transforms align tangentially with one of the two shear nets, while others rotate gradually to accommodate transitions between shear-dominated and kinematically dominated zones. This behavior is consistent with a stress-guided partitioning of deformation, in which plate kinematics operate within a pre-existing global stress architecture rather than independently of it.

Seismicity and volcanism further reinforce this interpretation. Earthquake epicenters ($M \geq 4.5$ over the past 25 years) cluster preferentially along shear-aligned corridors, particularly where shear trajectories curve sharply or converge. Active and historically active volcanoes similarly concentrate along these zones, indicating that magma ascent and fault reactivation are favored where the imposed stress field enhances strain localization. The coincidence of active deformation with predicted shear geometry is especially striking given the rapid tectonic evolution and high strain rates characteristic of the region.

Importantly, the Central America–Caribbean system illustrates how global shear geometry can remain legible even in environments dominated by plate-boundary processes. Rather than obscuring the shear pattern, the complexity of the region appears to amplify it, making the underlying geometric constraints more visible. This observation supports the broader conclusion that the global shear-net framework functions as an organizing template that biases the orientation, curvature, and longevity of tectonic features generated by plate interactions.

In summary, Central America and the Caribbean represent a high-strain, multi-plate environment in which the influence of a planet-scale shear architecture remains clearly expressed. The region bridges the behavior observed in stable continental interiors and that seen in highly active subduction systems, underscoring the robustness of the shear model across contrasting tectonic regimes.

3.5 South Indian Ocean Tectonic Arc

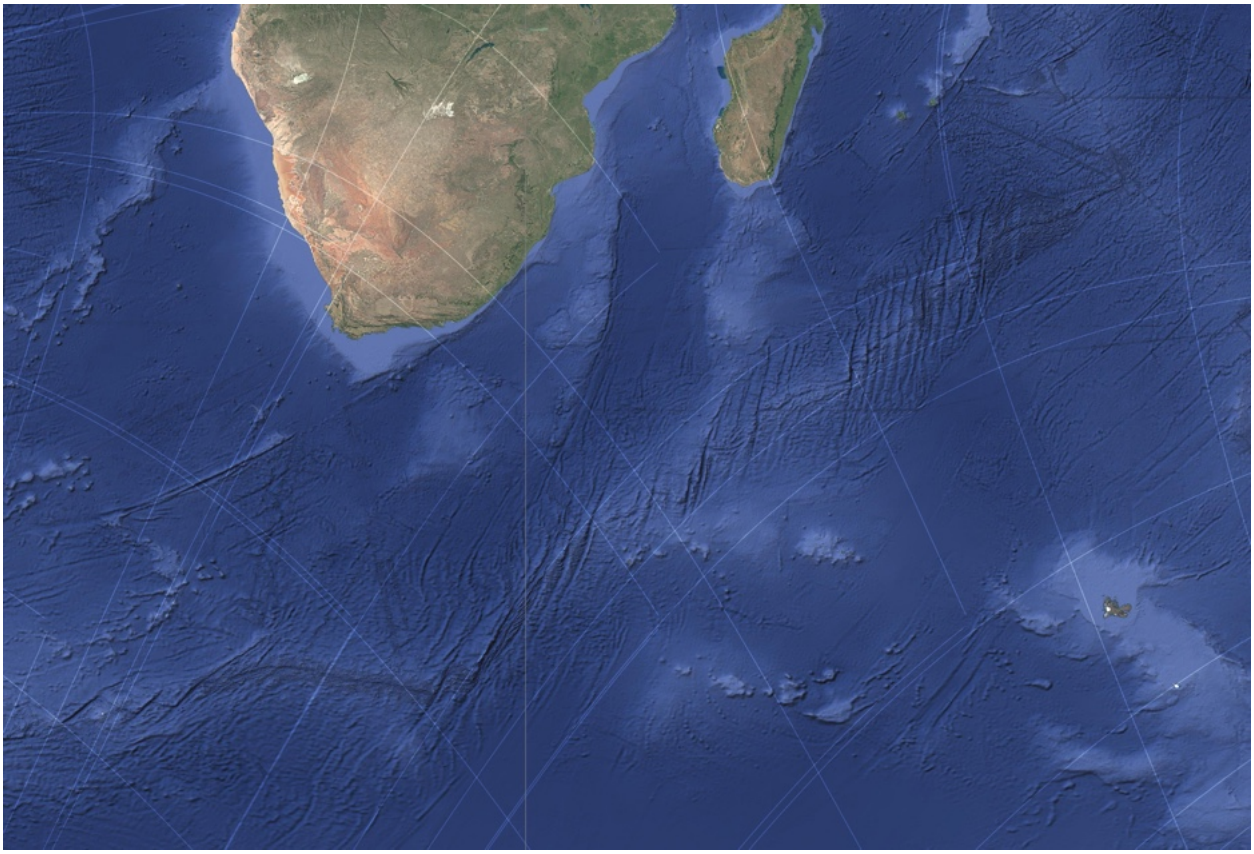

Figure 5: A vast tectonic arc in the southern Indian Ocean displaying strong congruence with modeled shear trajectories.

The southern Indian Ocean contains one of the least discussed yet most geometrically coherent arcuate tectonic features identified in this study. Extending across abyssal plains and intersecting multiple spreading systems, this arc has no widely accepted singular tectonic explanation, often being treated as a composite outcome of ridge propagation, transform segmentation, and inherited mantle structure. However, these mechanisms do not readily explain the smooth, large-radius curvature of the feature nor its persistence across regions of differing spreading histories.

Within the global shear-net framework, the South Indian Ocean arc aligns closely with invariant shear contours, occupying a region of minimal differential shear under the prescribed true polar wander geometry. This alignment is particularly significant because oceanic lithosphere is continuously regenerated; the preservation of curvature in such a setting implies that the stress geometry responsible for organizing the feature must be both long-wavelength and repeatedly imposed.

Bathymetric and gravity data reveal that ridge segments, fracture zones, and subtle topographic highs along the arc preferentially conform to the modeled curvature rather than to local spreading directions alone. In several locations, ridge axes rotate smoothly to remain approximately orthogonal to nearby shear trajectories, while transform offsets tend to parallel one of the shear nets. This

behavior mirrors that observed along the Mid-Atlantic Ridge and supports a common organizing mechanism.

The South Indian Ocean arc is particularly diagnostic because it lacks the complicating influence of continental inheritance. Its geometry must therefore arise from interactions between mantle flow, lithospheric accretion, and an imposed global stress field. In this context, the shear-net model provides a parsimonious explanation: ridge initiation, segmentation, and abandonment are biased by a persistent shear topology that modulates where and how oceanic lithosphere forms.

This interpretation also offers insight into the longevity of the arc. Even as spreading centers migrate and plate configurations evolve, the invariant shear geometry remains spatially fixed relative to the Earth, allowing successive generations of oceanic crust to inherit similar curvature. The result is a composite bathymetric signature that integrates stress over tens of millions of years.

In summary, the South Indian Ocean tectonic arc represents a purely oceanic manifestation of the global shear framework, free from continental overprint and therefore particularly compelling. Its correspondence with invariant contours strengthens the case that the modeled shear field reflects a real, long-lived component of Earth's stress architecture capable of influencing both continental and oceanic tectonics.

3.6 Sulawesi and Western Pacific Bathymetry

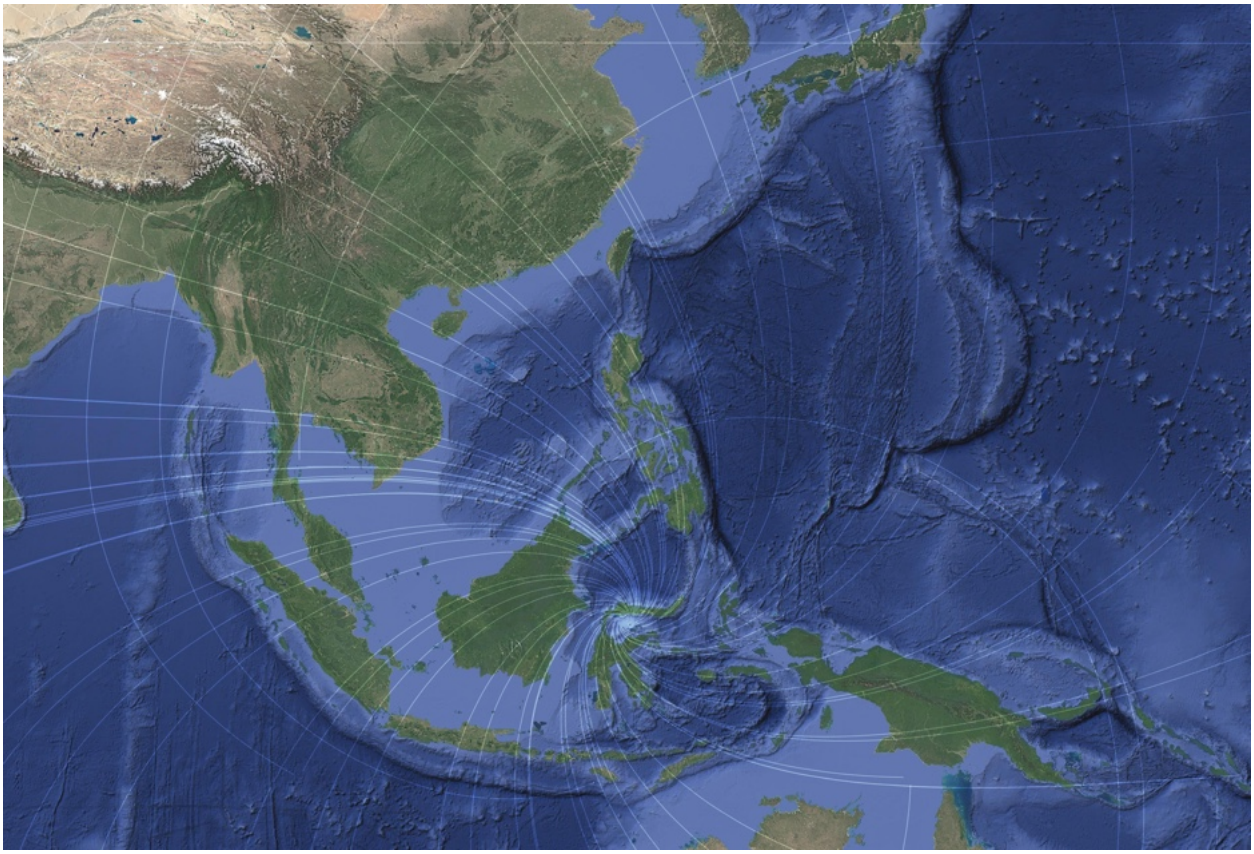

Figure 6: Primary and secondary bathymetric arcs near Sulawesi aligned with predicted shear trajectories.

The Sulawesi–Banda region represents one of the most structurally complex tectonic environments on Earth, characterized by tightly curved island arcs, deep bathymetric basins, rapid slab rollback, and intense seismic and volcanic activity. Conventional interpretations invoke a combination of microplate rotations, slab tearing, back-arc spreading, and variable subduction polarity to explain this complexity. While these mechanisms describe the kinematics, they do not fully explain the exceptional geometric coherence of the Banda Arc nor its nested, near-spiral morphology.

When examined in the context of the global shear-net model, the Banda Sea and surrounding arcs emerge as a textbook example of shear convergence and rotational confinement. Both Net 1 and Net 2 trajectories curve strongly into the region, producing a tightly wound shear vortex whose geometry closely mirrors the observed bathymetry, trench curvature, and volcanic arc alignment. The Banda Arc itself traces an almost perfect segment of an invariant contour, while subsidiary structures align alternately parallel and perpendicular to the local shear directions.

This configuration implies that the Sulawesi–Banda system occupies a zone of extreme shear focusing, where long-wavelength stress trajectories are forced into tight curvature by global bound-

ary conditions. In such a regime, even modest lithospheric heterogeneity or pre-existing weaknesses can be rapidly amplified into complex rotational tectonics. Rather than being the primary cause of curvature, microplate rotations may therefore be a mechanical response to an imposed stress geometry that favors angular momentum conservation within a confined domain.

Bathymetric features northeast of Sulawesi further reinforce this interpretation. Smaller arcuate basins and ridges exhibit scaled-down versions of the same geometric relationships seen in the Banda Arc, suggesting a fractal or self-similar expression of the underlying shear field. These features are difficult to reconcile with isolated slab dynamics but arise naturally if the lithosphere is responding to a continuous, globally imposed stress network.

The spatial coincidence of dense seismicity and active volcanism with zones of maximum shear curvature provides additional support. Earthquake hypocenters cluster along shear-aligned trajectories, while volcanic centers preferentially occupy regions where shear transitions from compressional to extensional regimes. This pattern is consistent with stress-driven melt focusing and fault reactivation governed by shear geometry rather than by plate boundaries alone.

In this framework, the Sulawesi–Banda system represents an end-member case of rotational tectonics driven by global shear confinement. Its extreme curvature is not anomalous, but rather the expected outcome when a mobile lithospheric domain is embedded within a high-curvature segment of a planetary-scale stress field. The apparent complexity of the region thus reflects the clarity with which the underlying shear architecture is expressed, making Sulawesi–Banda one of the most diagnostically valuable natural laboratories for evaluating global stress models.

3.7 Mid-Atlantic Ridge

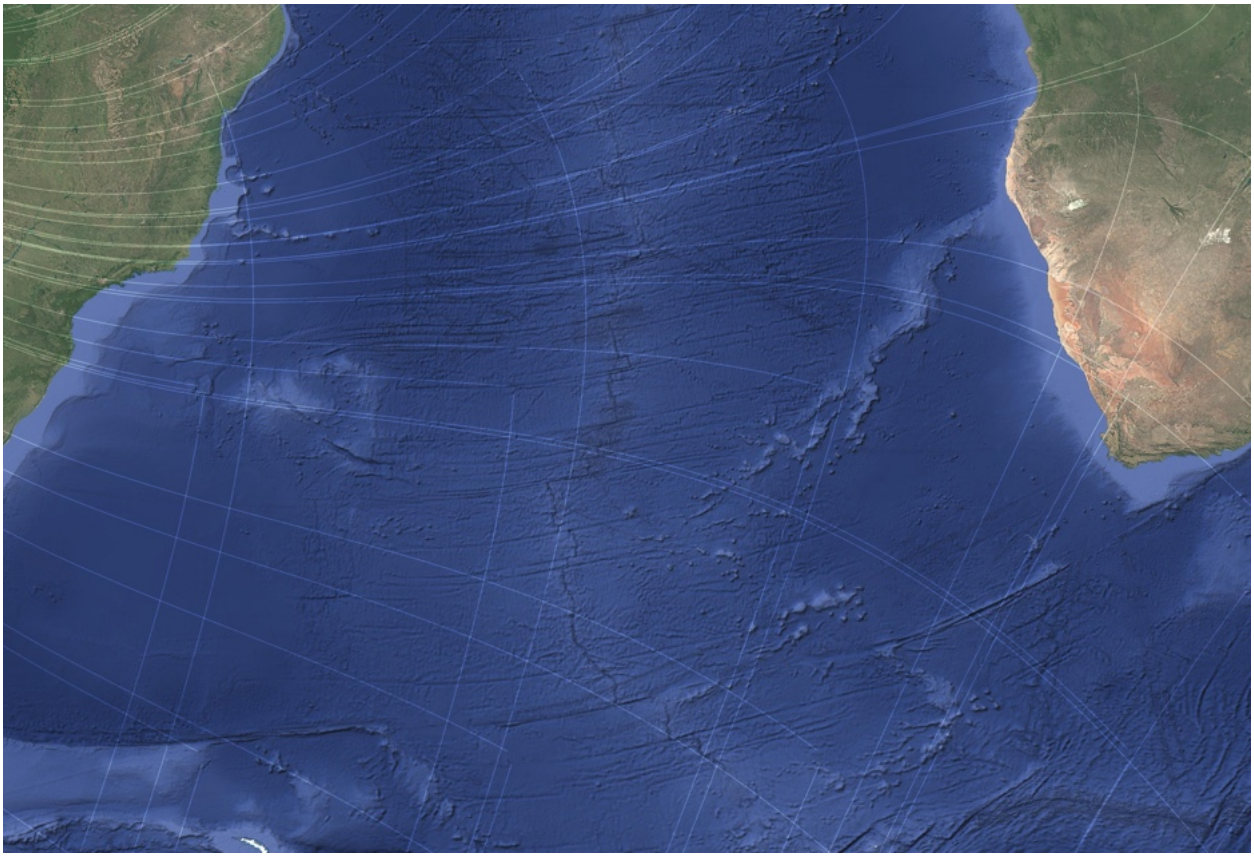

Figure 7: The Mid-Atlantic Ridge exhibits alternating alignment with Net 1 and Net 2 shear families along strike.

The Mid-Atlantic Ridge (MAR) provides a uniquely powerful test of the global shear-net framework because it is an actively forming plate boundary where lithosphere is continuously created. Any persistent geometric alignment in such a setting must therefore reflect ongoing boundary conditions rather than fossil inheritance alone. While the MAR is conventionally interpreted as a passive response to divergent plate motion modulated by mantle upwelling and transform segmentation, this view does not fully account for the systematic alternation in ridge orientation and segmentation observed along its length.

When compared with the modeled global shear field, the MAR exhibits a striking pattern of alternating alignment with Net 1 and Net 2 trajectories. Rather than maintaining a single preferred orientation, ridge segments rotate gradually to remain approximately orthogonal to the dominant local shear direction, while intervening transform faults tend to align parallel to the complementary net. This alternating behavior repeats quasi-periodically from the North Atlantic through the equatorial region and into the South Atlantic.

Such systematic alternation is difficult to reconcile with local spreading-rate variations or

stochastic mantle heterogeneity alone. In contrast, it arises naturally if ridge orientation is biased by a persistent, long-wavelength shear topology that operates alongside plate divergence. In this framework, spreading occurs most efficiently where ridge axes are orthogonal to maximum shear gradients, while transform offsets develop preferentially along shear-parallel orientations that minimize resistance to lateral motion.

The MAR also demonstrates how global shear geometry can coexist with, rather than oppose, plate tectonic processes. Plate divergence supplies the kinematic requirement for spreading, while the shear field constrains how that spreading is geometrically expressed. This explains why the MAR maintains a coherent, planet-scale sinuosity despite changes in spreading rate, ridge propagation, and segment lifespan.

Importantly, the alternation observed along the MAR mirrors behavior seen in continental rift systems, such as the East African Rift, and in oceanic arcs, such as those of the southern Indian Ocean. This consistency across tectonic regimes reinforces the interpretation that the shear-net framework captures a fundamental aspect of Earth's stress organization, rather than a feature peculiar to any single environment.

In summary, the Mid-Atlantic Ridge demonstrates that the global shear field is not merely a fossil imprint preserved in ancient lithosphere, but an active geometric constraint influencing present-day plate boundary evolution. Its alternating alignment with the two shear nets provides one of the clearest indications that long-wavelength planetary stress fields continue to operate alongside, and in coordination with, plate tectonic processes.

3.8 North American Arcuate Lake Chain

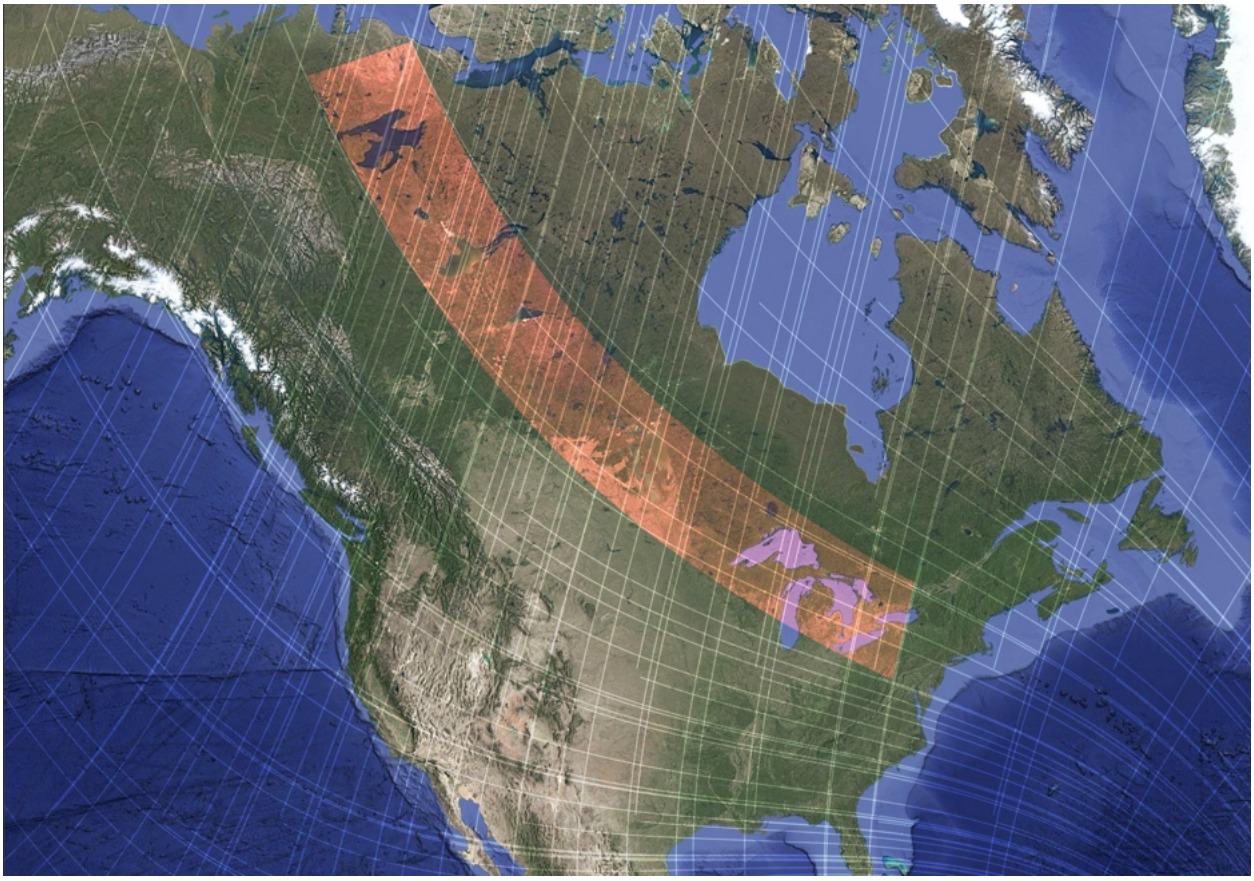

Figure 8: A continental-scale arc of large lakes across North America aligned with invariant shear contours.

Across central and eastern North America, a prominent northwest–southeast–trending arc of large lakes extends from the Canadian Shield through the Great Lakes region and into the northeastern United States. This sequence includes, but is not limited to, Great Bear Lake, Great Slave Lake, Lake Winnipeg, Lake Superior, Lake Michigan, Lake Huron, Lake Erie, and Lake Ontario, together with numerous subsidiary basins embedded within the Shield. Conventional explanations emphasize glacial excavation of pre-existing basins and selective erosion along lithological boundaries. While glaciation clearly played a decisive role in shaping lake morphology, it does not satisfactorily explain the large-scale arcuate coherence, continuity across cratonic blocks, or the repeated correspondence between basin margins and deep structural fabrics.

When examined in the context of the global shear-net model, this lake arc aligns closely with one of the dominant shear trajectories, with local modulation where the secondary net intersects. The resulting geometry is not linear but gently curvilinear, matching the modeled stress paths rather than simple plate-boundary or rift-parallel trends. This correspondence persists across multiple tectonic provinces, including Archean cratons, Proterozoic orogens, and Phanerozoic sedimentary

basins, indicating control by a stress field that transcends individual geological episodes.

Lake Superior provides a particularly instructive case. Its elongated, asymmetric basin follows a shear-aligned trajectory that intersects the Midcontinent Rift at a high angle. Although the rift supplied structural weakness and magmatic thickening, the ultimate basin geometry appears to reflect superposed shear rather than pure extensional control. Similar relationships are observed in Lakes Michigan and Huron, whose orientations deviate from local stratigraphic trends but conform closely to the modeled net.

Further north, the large arcuate basins of Great Bear and Great Slave lakes occupy regions of distributed shear convergence near the Fort Simpson Arc. These lakes lie at the interface between stable cratonic lithosphere and reworked Proterozoic belts, where shear-induced strain localization would be expected to produce broad, shallow depressions rather than narrow rift valleys. The continuity of lake orientation across this transition supports a tectonic origin rooted in long-wavelength stress organization rather than isolated rifting events.

Glaciation acted as an efficient excavator of these preconditioned zones, preferentially deepening basins aligned with shear-parallel weaknesses. The repeated occupation of these pathways by ice streams further amplified relief and connectivity, but did not generate the underlying geometry. This interpretation is reinforced by the observation that many lake margins coincide with bedrock lineaments, gravity anomalies, and seismic discontinuities that predate the last glacial maximum by hundreds of millions of years.

Collectively, the North American arcuate lake systems can be interpreted as surface expressions of a persistent, continent-scale shear fabric imposed episodically through geological time. Their coherence provides independent support for the existence of a globally organized stress field capable of imprinting large-scale curvature onto otherwise stable continental interiors. Rather than anomalous features requiring ad hoc explanations, these lakes emerge naturally from the interaction between long-lived shear geometry and episodic erosional amplification.

3.9 United Kingdom Bimodal Morphology

Figure 9: Bimodal geomorphic orientation in the United Kingdom, particularly Scotland, aligned with both shear families.

The British–Irish Isles exhibit a strikingly bimodal geomorphological and structural fabric that has long been recognized but remains only partially explained within conventional tectonic frameworks. Standard interpretations emphasize Caledonian and Variscan orogenesis, later reactivation during Atlantic rifting, and extensive modification by Pleistocene glaciation. While each of these processes contributed materially to the present landscape, none adequately accounts for the persistent, large-scale directional coherence observed across disparate lithologies, ages, and tectonic provinces.

When overlaid with the global shear-net model, the United Kingdom occupies a region where Net 1 and Net 2 trajectories intersect at moderate angles, producing a dual stress fabric that is clearly expressed in topography, drainage patterns, and bedrock structure. This bimodality is particularly evident in Scotland, where major lineaments, fjord systems, loch orientations, and mountain ranges alternate between alignments parallel to each net. The Highlands, Grampians, and Northern Isles collectively preserve a directional memory that transcends individual orogenic episodes.

Scotland provides the clearest exposure of this geometry due to limited sedimentary cover

and extensive glacial stripping, which has preferentially excavated along pre-existing shear-aligned weaknesses. The resulting landscape acts as a natural strain gauge, revealing the orientation of mechanically favored planes. Notably, many glacial valleys and sea lochs exploit structures that are oblique to known Caledonian thrusts yet closely parallel to modeled shear trajectories, suggesting reactivation under later stress regimes rather than simple inheritance from early Paleozoic deformation.

England and Wales, though more subdued topographically, retain the same dual orientation in river networks, escarpments, and basin margins. The Pennine spine, the Welsh uplands, and the structural grain of southern England collectively reflect alternating shear control, even where tectonic activity has been minimal since the Mesozoic. Ireland displays comparable behavior, with major basins, coastal embayments, and lineament systems aligning with the same two dominant stress directions.

This bimodal expression implies that the British–Irish lithosphere has repeatedly experienced stress fields aligned with the global shear geometry, leading to cumulative reinforcement of specific orientations through multiple tectonic and climatic cycles. Rather than being overprinted or erased, earlier structures were selectively reactivated when favorably oriented relative to the imposed shear field, producing the observed persistence.

Importantly, this interpretation reframes glaciation as an amplifying rather than primary agent. Ice flow preferentially followed mechanically weakened, shear-aligned pathways, enhancing relief along these directions without dictating them. The strong correspondence between shear trajectories and geomorphology therefore reflects tectonic preconditioning rather than purely erosional sculpting.

In summary, the United Kingdom and Ireland represent a mid-latitude example of distributed shear expression, where neither net dominates entirely. The resulting bimodal morphology provides compelling evidence that long-wavelength, globally coherent stress fields can exert durable control over regional landscape evolution, even in tectonically quiescent settings.

3.10 East African Rift System

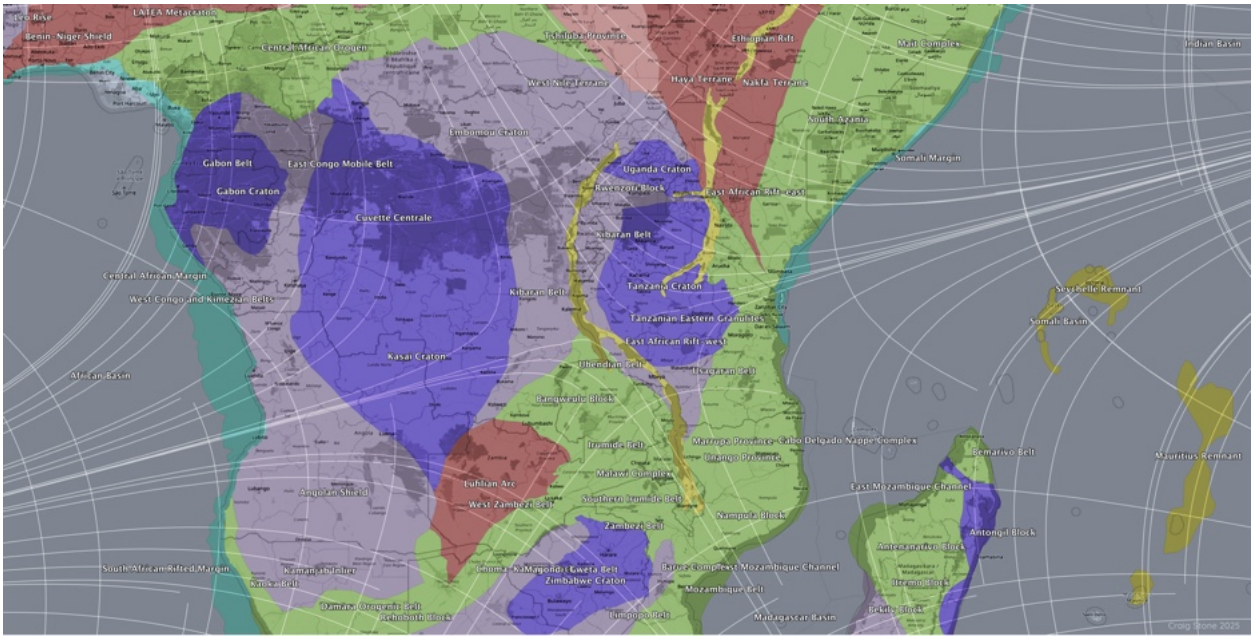

Figure 10: Double-arc geometry of the western East African Rift coincident with convergence of Net 1 and Net 2 near 14°S, 31°E.

The East African Rift System (EARS) has long been interpreted as a classic example of continental rifting driven by mantle upwelling, lithospheric thinning, and plate-boundary reorganization. While this framework explains the broad extensional regime, it does not fully account for the pronounced arcuate geometry of the rift system, nor for the existence of two parallel, partially overlapping rift branches that curve coherently across multiple tectonic provinces.

Within the global shear-net model, the East African Rift occupies a region of marked convergence between Net 1 and Net 2 trajectories, centered near approximately 14°S, 31°E. This location corresponds closely to the intersection of the eastern and western rift branches, where deformation transitions from distributed extension to focused rifting and volcanism. The resulting geometry naturally produces paired arcuate structures rather than a single linear rift, consistent with observations.

The western branch of the rift, in particular, traces a smooth arc that aligns closely with one family of shear trajectories, while the eastern branch exhibits alternating alignment between the two nets. This dual behavior mirrors the broader bimodal stress configuration predicted by the model and provides a geometric explanation for the long-standing asymmetry between the two branches. Rather than representing independent rifting events, the paired arcs can be interpreted as complementary responses to the same imposed stress field acting on lithosphere with variable thickness and rheology.

Volcanic centers and zones of elevated seismicity cluster preferentially along regions of shear

convergence and curvature change. These locations correspond to areas where the modeled shear field predicts enhanced strain localization and rotational stress gradients, conditions favorable for magma ascent and fault reactivation. The spatial association between volcanism, seismicity, and shear geometry persists across both Precambrian cratons and younger mobile belts, underscoring the independence of the pattern from local lithologic control.

The longevity of the East African Rift further supports this interpretation. Episodes of rifting, magmatism, and basin formation have recurred intermittently since at least the Paleogene, yet the large-scale curvature and branch geometry have remained remarkably stable. Such persistence is consistent with repeated reactivation of a pre-existing shear-guided lithospheric architecture rather than with transient plume-driven extension alone.

In this framework, mantle upwelling and thermal weakening act as facilitators rather than primary architects of rift geometry. The global shear field establishes the orientation, curvature, and segmentation of deformation, while buoyancy-driven processes supply the energy required to exploit these mechanically favorable pathways. The East African Rift thus emerges as a continental-scale analogue to other double-arc systems identified in this study, reinforcing the view that long-wavelength planetary stress fields exert a fundamental influence on the organization of extensional tectonics.

3.11 Greenland, Hudson Bay, and the Nastapoka Arc

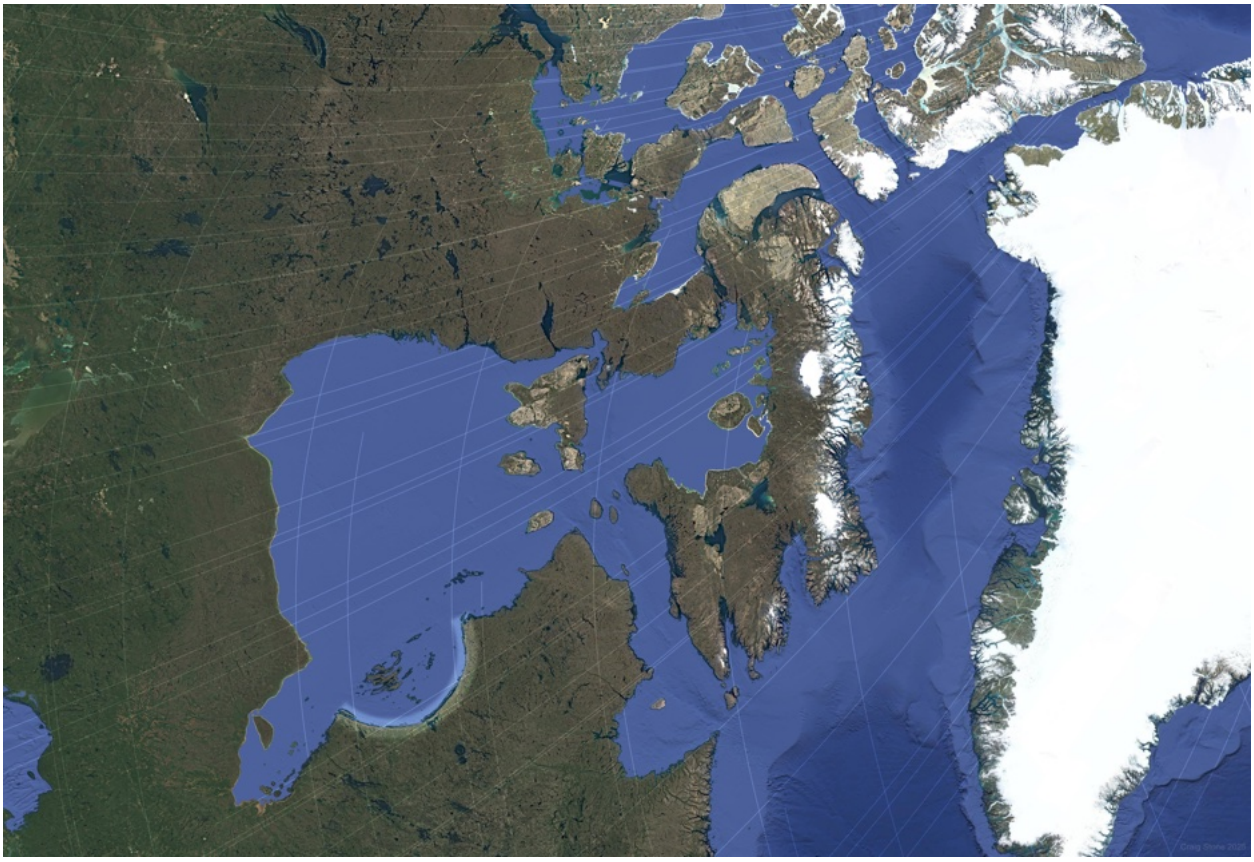

Figure 11: Greenland and Hudson Bay in polar stereographic projection showing bimodal agreement with shear nets and the arcuate Nastapoka structure.

High-latitude regions provide a stringent test for global stress models because projection artifacts are minimized in polar views and because cratonic lithosphere dominates over young plate-boundary deformation. When examined in polar stereographic and orthographic projections, Greenland, Hudson Bay, and the Nastapoka Arc exhibit some of the clearest and least ambiguous expressions of the global shear-net framework identified in this study.

Greenland displays a pronounced bimodal structural and geomorphic fabric that aligns closely with both Net 1 and Net 2 trajectories. Fjord systems, coastal embayments, and interior lineaments alternate systematically between the two shear orientations. This bimodality is evident even beneath extensive ice cover, as revealed by subglacial topography and bedrock structure, indicating that the geometry is inherited from deep lithospheric architecture rather than imposed by surface processes. The coherence of this pattern across Greenland's Archean craton and Proterozoic margins suggests long-term preservation of shear-aligned weakness zones.

Hudson Bay occupies a particularly significant position within the shear framework. Its near-circular to weakly polygonal outline coincides with a region of shear convergence and minimal

differential stress, consistent with an invariant or low-strain node in the modeled field. Such locations are expected to favor long-term subsidence, thermal relaxation, or crustal thinning without strong directional deformation. This provides a compelling geometric explanation for the persistence of Hudson Bay as a large, shallow basin despite repeated glaciation, isostatic rebound, and regional tectonic quiescence.

The Nastapoka Arc, forming the southeastern margin of Hudson Bay, is among the most precise large-scale arcuate features preserved in continental crust. Its curvature, continuity, and length closely mirror nearby invariant shear contours and remain remarkably undisturbed across multiple geological provinces. While impact hypotheses have occasionally been proposed, the absence of unequivocal shock features and the arc's conformity with broader continental stress geometry favor an interpretation rooted in inherited lithospheric structure. Within the shear-net framework, Nastapoka represents a segment of a long-lived shear-guided curvature that has been selectively exposed and sharpened by glacial erosion rather than created by it.

Importantly, the Greenland–Hudson Bay–Nastapoka system mirrors other arcuate features identified in this study, including the Himalayan arc, the Banda Arc, and the southeastern North American sediment belt. In each case, large-radius curvature corresponds to regions of stable shear geometry rather than to localized forcing mechanisms. The recurrence of this pattern across both hemispheres and across vastly different tectonic settings argues strongly for a common organizing principle.

In this interpretation, glaciation acts primarily as a revealing agent, preferentially eroding along mechanically weakened, shear-aligned zones and thereby enhancing the visibility of inherited curvature. The exceptional clarity of the Arctic examples reflects the combined effects of cratonic rigidity, minimal sedimentary cover, and repeated erosional stripping, which together preserve the imprint of global-scale stress with minimal overprinting.

Taken together, Greenland, Hudson Bay, and the Nastapoka Arc provide some of the most compelling evidence that the global shear-net framework captures a real and persistent aspect of Earth's lithospheric organization. Their geometry cannot be readily attributed to isolated tectonic, impact, or climatic processes, but emerges naturally from a long-wavelength, planet-scale stress architecture operating over geological time.

3.12 Northwestern Canada and the Fort Simpson Arc

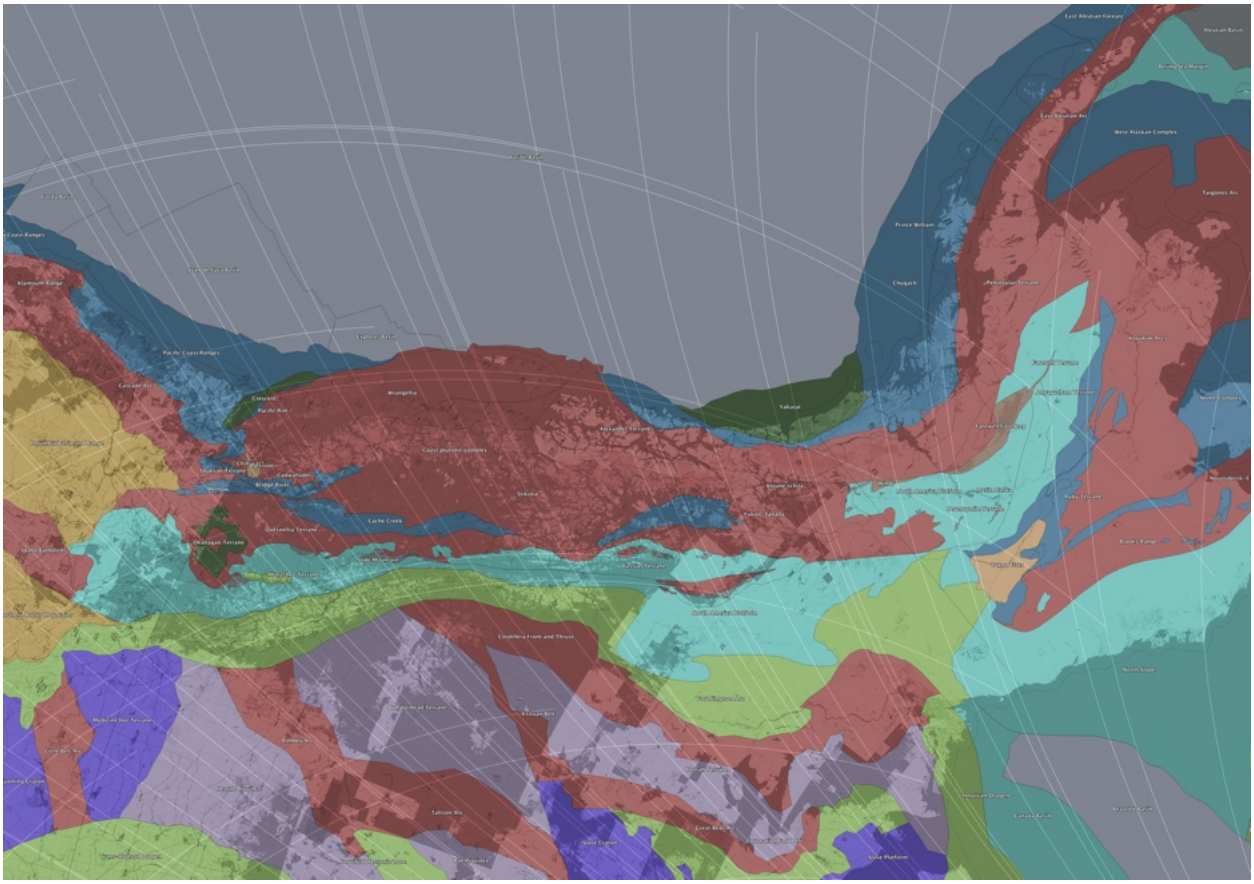

Figure 12: Northwestern Canada showing multiple agreements with shear nets, including the Fort Simpson Arc and transition from the Coast Plutonic Complex to the East Aleutian Arc.

The Fort Simpson Arc anomaly (FSA) of northwestern Canada has traditionally been interpreted as an Early Proterozoic magmatic arc, based on its curvilinear aeromagnetic signature, associated positive gravity anomalies, and U–Pb zircon ages clustering near ∼1.85 Ga from granitoid basement exposures. This interpretation, while well supported by geochronological and petrological evidence, encounters several persistent geometric and tectonic ambiguities that warrant re-examination in light of the global shear-net framework developed here.

Previous syntheses note that the Fort Simpson anomaly is not a simple linear feature, but instead broadens and curves westward into large elliptical magnetic highs near Great Bear Lake, among the most extensive aeromagnetic features in North America. Even within conventional interpretations, these western highs are acknowledged as potentially distinct basement elements that appear unified only through filtered geophysical datasets. Moreover, the Fort Simpson domain exhibits a long history of reactivation, influencing later extensional basins, dyke swarms, hydrothermal systems, and lithospheric segmentation over a time span exceeding one billion years.

When examined in polar and Arctic projections, the Fort Simpson Arc displays a close geometric

correspondence with one of the principal branches of the modeled global shear net. In particular, the curvature, bifurcation, and apparent bimodality of the Fort Simpson structure coincide with zones of net convergence and rotation in the shear trajectories. This correspondence is independent of stratigraphic boundaries, terrane affinities, or magmatic age constraints, suggesting a kinematic control that predates and outlasts any single tectono-magmatic episode.

Within this framework, Early Proterozoic arc magmatism is reinterpreted not as the origin of the Fort Simpson structure, but as one expression of a pre-existing lithospheric shear corridor. Such corridors are expected to localize mantle upwelling, magma ascent, and crustal underplating during periods of favorable stress orientation, while remaining mechanically weak and prone to reactivation under subsequent stress regimes. The coincidence of the Fort Simpson anomaly with positive gravity signatures is consistent with shear-focused lower-crustal densification or mafic underplating, rather than requiring a uniquely arc-related mechanism.

This reinterpretation resolves several longstanding difficulties associated with an arc-only model. The pronounced curvature and elliptical geometry of the Fort Simpson anomaly, its apparent continuity despite internal geological heterogeneity, and its repeated reactivation through Proterozoic and Phanerozoic time are all natural consequences of long-lived lithospheric shear structures, but are atypical of transient subduction-related arcs. Importantly, this perspective does not negate the arc-related geochemical and geochronological evidence documented in earlier studies; rather, it reframes arc magmatism as a secondary response to an inherited stress architecture.

In this view, the Fort Simpson Arc anomaly represents a lithospheric-scale shear feature that has acted as a persistent organizer of deformation and magmatism since at least the Paleoproterozoic. Its alignment with the global shear net supports the broader hypothesis that certain first-order continental geological features are governed by planet-scale kinematic patterns associated with large-amplitude true polar wander, rather than by isolated plate-boundary processes alone.

—

4 Global Plate Boundary Comparison

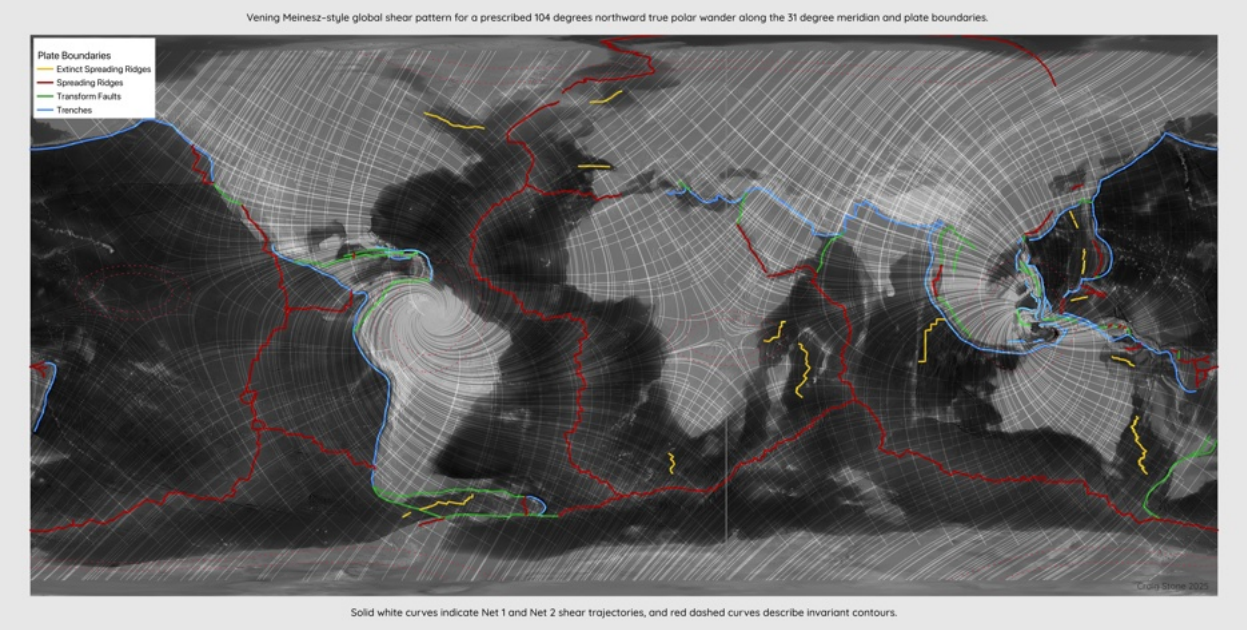

Figure 13: Comparison of the global shear model with modern plate boundaries. Strong geometric correspondence is observed across subduction arcs, transforms, and extinct ridges.

—

4.1 Comparative Behaviour of the Two Euler-Point Domains

The two Euler-point regions defined by the prescribed 104° northward true polar wander (TPW) along the 31°E meridian provide a natural experiment for evaluating how the modeled global shear field couples into contrasting tectonic environments (Figures 14 and 15). Although both regions exhibit clear correspondence with the Venning–Meinesz–style shear trajectories, the mode of conformance differs in ways that are geologically informative.

Western Euler Domain. The western Euler point, centered over northern South America and the Caribbean (Figure 14), exhibits the strongest and most internally consistent agreement between the shear model and observed geology. In this domain, shear trajectories form tightly wrapped spiral patterns that closely parallel Precambrian cratonic margins, mobile belts, and long-lived deformation zones. Major rift and transform boundaries, earthquake epicenter distributions ($M \geq 4.5$ over the past 25 years), and active to historically active volcanic centers preferentially align tangentially to the modeled shear flow.

Notably, both ancient tectonic fabrics and present-day deformation are organized predominantly along shear-parallel trajectories rather than orthogonal to them. This indicates that the shear field has acted as a persistent organizing stress over multiple tectonic cycles, repeatedly reactivating

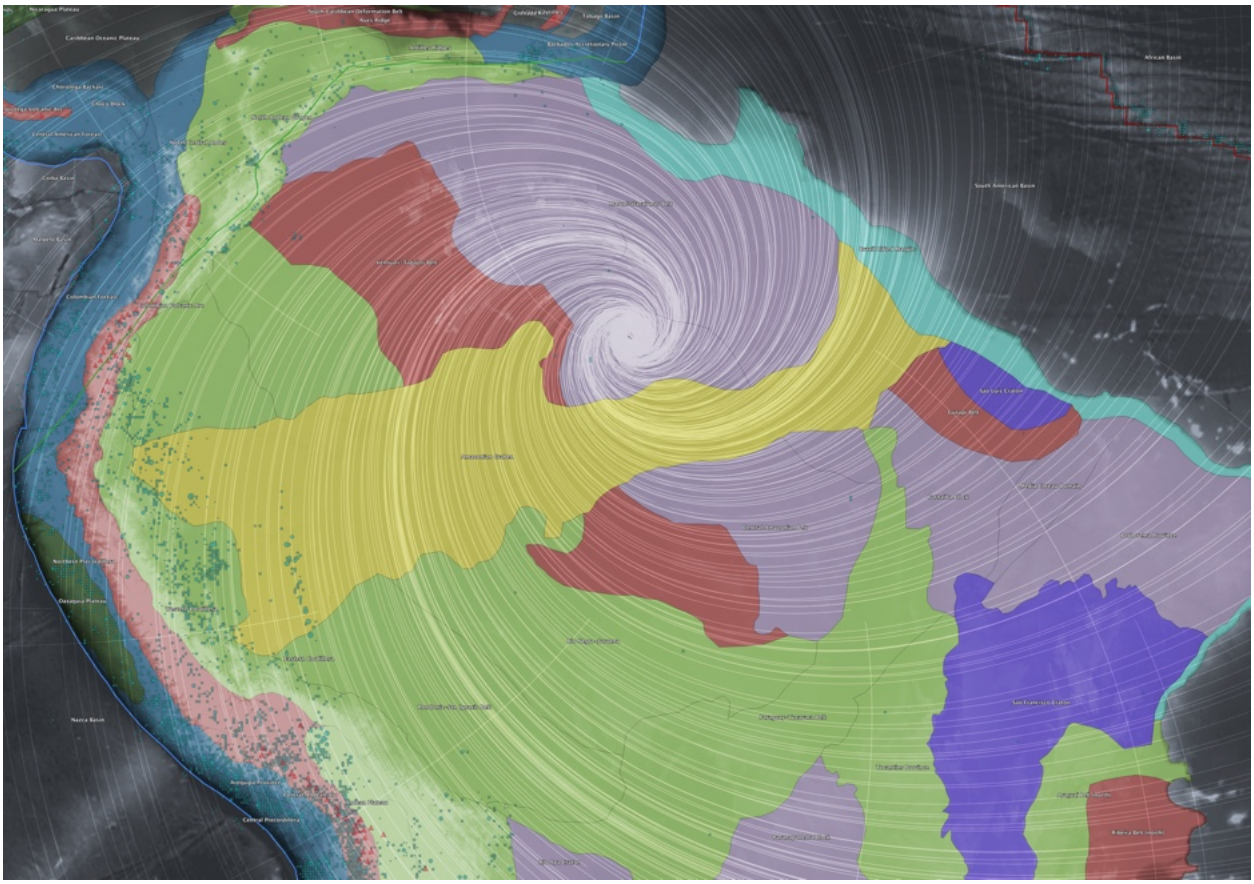

Figure 14: Western Euler-point domain showing the Venning–Meinesz–style shear trajectories overlaid on geological provinces, plate boundaries, earthquake epicenters (M≥4.5), and volcanic centers.

inherited lithospheric weaknesses in geometrically consistent orientations. The high degree of spatial coherence suggests that thick, mechanically heterogeneous continental lithosphere is capable of preserving and expressing low-order global stress modes over geological timescales.

Eastern Euler Domain. The eastern Euler point, located within the Indonesia–Sunda–Banda tectonic collage (Figure 15), presents a contrasting but equally informative expression of the same underlying shear structure. This region is characterized by rapid plate convergence, slab rollback, arc–continent collision, and distributed back-arc deformation. Despite this complexity, several robust correspondences with the shear model remain evident.

Major arcuate subduction systems, including the Banda and Sunda arcs, follow curvature consistent with modeled shear trajectories rather than simple relative plate-motion vectors. Earthquake hypocenters cluster along curved bands that mirror regions of maximum shear curvature, while active and historical volcanism preferentially occupies shear-aligned arc segments and convergence zones. In this domain, rift boundaries and basin margins exhibit mixed behavior: some conform closely to shear trajectories, whereas others are dominated by local slab geometry and rollback dynamics. This indicates that while the shear field does not dictate tectonic behavior outright, it

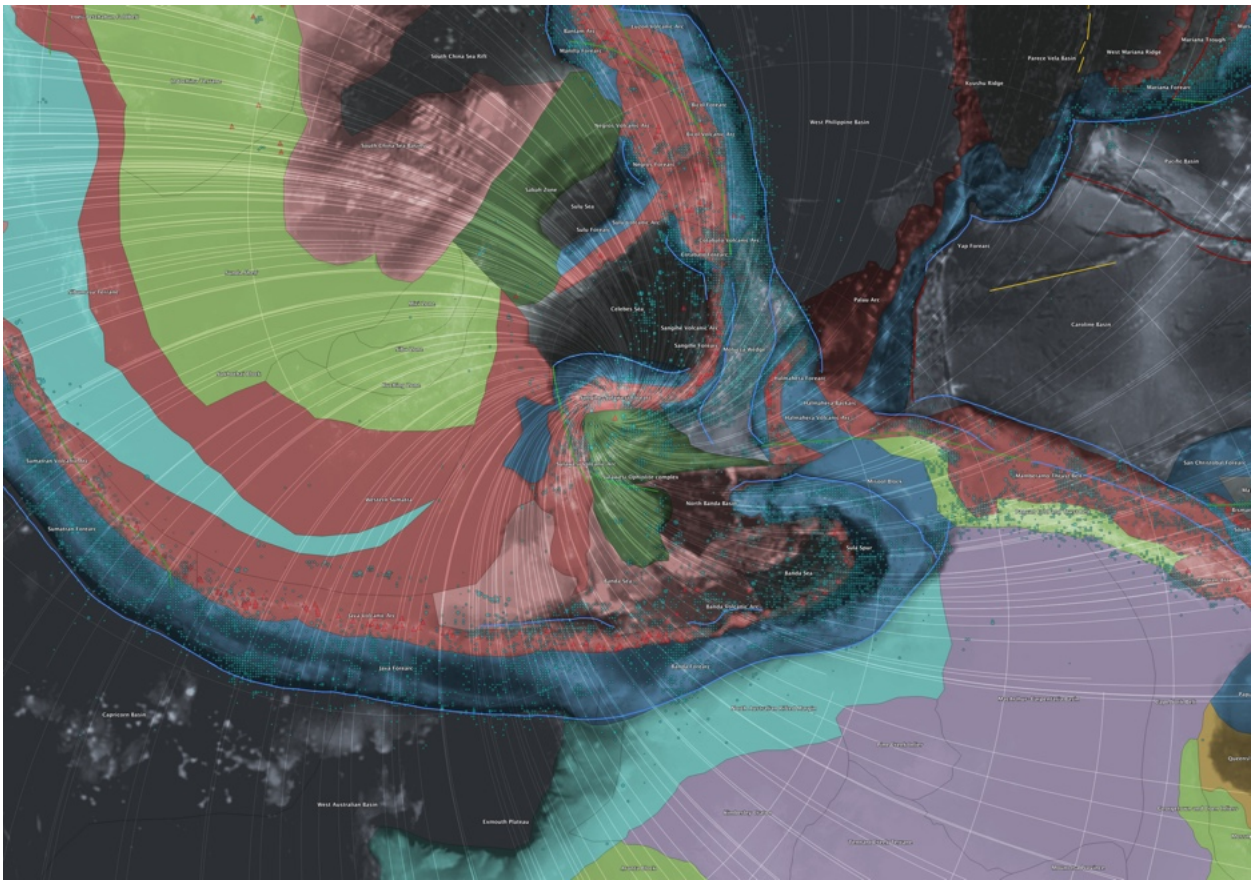

Figure 15: Eastern Euler-point domain (Indonesia–Sunda–Banda region) illustrating the relationship between modeled shear trajectories, arcuate subduction systems, seismicity, and active volcanism.

acts as a geometric constraint within which subduction-driven processes organize themselves.

Comparative Implications. The contrasting behavior of the two Euler domains highlights several important implications. First, the persistence of recognizable shear conformance in both stable continental interiors and highly active subduction zones argues against coincidental alignment and supports the presence of a global, low-order stress architecture capable of coupling into diverse lithospheric contexts. Second, regions underlain by thick, ancient lithosphere appear to preserve shear-imposed geometry more faithfully than rapidly recycling convergent margins, emphasizing the role of lithospheric memory in amplifying the visibility of the shear field.

Finally, the results indicate that the modeled shear structure should be understood not as a replacement for plate tectonics or mantle convection, but as a superimposed, long-wavelength stress mode that biases the orientation, curvature, and persistence of tectonic features generated by those processes. The systematic differences observed between the western and eastern Euler-point domains therefore strengthen the interpretation that the Venning–Meinesz–style global shear field represents a persistent and physically meaningful component of Earth's geodynamic system.

5 Scale-Dependent Spatial Autocorrelation of the Misfit Field

Permutation-based spatial autocorrelation analysis was applied to the stress–misfit field to quantify the degree and spatial extent of geographic organization across multiple length scales. Global Moran's I was computed using distance-weighted neighborhoods with characteristic scales of 250, 500, 1000, 2000, and 3000 km. Statistical significance was assessed using permutation-based null models in which misfit values were randomly reassigned to spatial locations while preserving the sampling geometry and marginal distribution.

5.1 Short-Wavelength Structure (250 km)

At a spatial scale of 250 km, the misfit field exhibits very strong positive spatial autocorrelation, with Moran's $I = 0.30$. The permutation null distribution has a mean effectively indistinguishable from zero and extremely small variance, yielding $p \ll 10^{-6}$. This result confirms that misfit values are highly clustered at short wavelengths and establishes a robust baseline of spatial coherence. At this scale, clustering is expected to reflect dominant local and regional tectonic controls, including fault systems, plate boundary geometry, and lithospheric heterogeneity.

5.2 Regional-Scale Coherence (500 km)

At 500 km, Moran's I remains large ($I = 0.23$) and highly significant under permutation testing ($p \ll 10^{-6}$). The reduction in Moran's I relative to 250 km reflects the expected decay of spatial correlation with distance, while the persistence of strong autocorrelation demonstrates that stress–misfit organization extends well beyond strictly local interactions. This scale corresponds to regional tectonic domains and large plate-boundary systems, indicating coherent stress structure at continental scales.

5.3 Long-Wavelength Organization (1000 km)

At a spatial scale of 1000 km, the misfit field continues to exhibit strong and statistically significant spatial autocorrelation, with Moran's $I = 0.17$ and $p \ll 10^{-6}$. The persistence of coherent structure at this wavelength exceeds typical crustal or single-orogen length scales and points to long-wavelength organization of the stress field. At this scale, purely local tectonic explanations become increasingly implausible, suggesting the influence of broader lithospheric or mantle-scale processes.

5.4 Planetary-Scale Persistence (2000 km)

At the largest scale examined, 2000 km, Moran's I remains positive and highly significant ($I = 0.11$, $p \ll 10^{-6}$). Although reduced in magnitude relative to shorter scales, the continued presence of statistically robust spatial autocorrelation at near-planetary wavelengths demonstrates that the

stress–misfit field is organized over distances comparable to hemispheric dimensions. This result rules out explanations confined to regional tectonics alone and establishes a minimum correlation length of at least several thousand kilometers.

5.5 Near-Hemispheric Spatial Coherence (3000 km)

At a spatial scale of 3000 km, the stress–misfit field continues to exhibit statistically robust positive spatial autocorrelation, with Moran's $I = 0.073$. Permutation-based null testing yields a null expectation indistinguishable from zero and an extremely small variance, resulting in $p \ll 10^{-6}$. Although the magnitude of Moran's I is reduced relative to shorter wavelengths, its persistence at this scale demonstrates coherent organization of the misfit field at near-hemispheric dimensions.

When considered alongside results at 250, 500, 1000, and 2000 km, the 3000 km analysis completes a smooth, monotonic decay of Moran's I across nearly an order of magnitude in spatial scale. No abrupt cutoff or loss of significance is observed. Such behavior is characteristic of a genuine long-wavelength correlation process rather than sampling artifacts or purely local tectonic interactions.

Spatial coherence at $\sim$3000 km exceeds the scale of individual plate interiors, major orogenic systems, and typical regional stress-transfer mechanisms. Instead, it implies the presence of organizing influences operating at planetary scales, such as mantle-wide stress transmission, low-degree spherical harmonic structure, or inertial reorganization of the lithosphere. While this analysis does not uniquely identify a causal mechanism, it establishes a minimum correlation length for the stress–misfit field that approaches hemispheric dimensions and cannot be explained by regional tectonics alone.

5.6 Scale Dependence and Correlation Length

Taken together, the results reveal a smooth, monotonic decay of Moran's I with increasing spatial scale, without loss of statistical significance across the full range examined (250–3000 km). Such behavior is characteristic of a genuine spatial correlation process with a long correlation length, rather than noise or sampling artifacts. The absence of a sharp cutoff indicates that the organizing mechanism operates across multiple spatial regimes, from local tectonic structure to global-scale stress organization.

5.7 Summary of Empirical Findings

The permutation-based spatial autocorrelation analysis demonstrates that the stress–misfit field is not spatially random at any examined scale. Instead, it exhibits strong and statistically robust geographic organization from local (250 km) through planetary (2000 km) wavelengths. These findings provide quantitative evidence for long-wavelength structure in the stress field and motivate

interpretation in terms of global or mantle-coupled forcing mechanisms, which are explored in the Discussion.

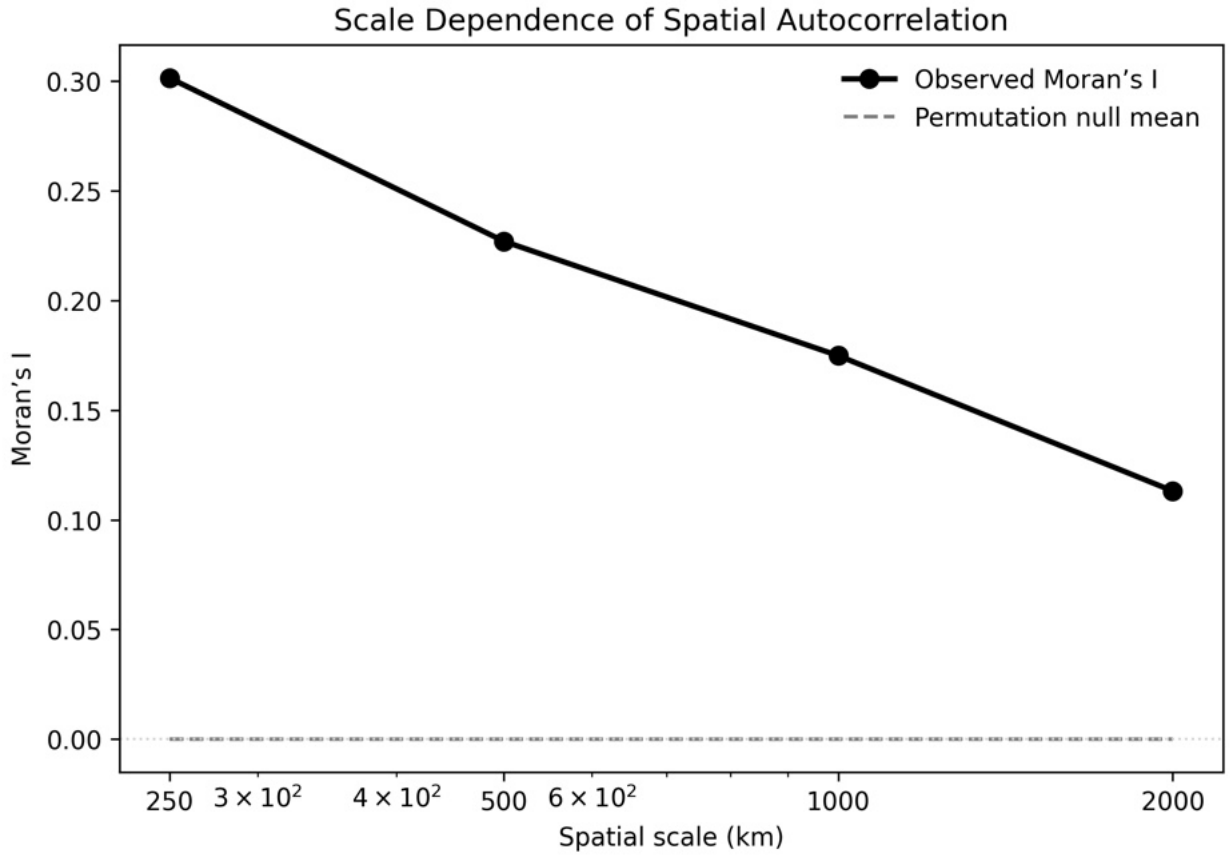

Figure 16: Spatial autocorrelation testing of shear–stress misfit using Moran's I. Angular misfit between observed maximum horizontal stress orientations from the World Stress Map (WSM) and modeled shear trajectories was computed at each observation site. Spatial autocorrelation was quantified using Moran's I with distance-decay weighting at multiple characteristic length scales (250, 500, 1000, and 2000 km). For each scale, a permutation-based null model (1000 realizations) was generated by randomly shuffling misfit values among spatial locations while preserving the spatial sampling geometry. Observed Moran's I values were compared to the null distributions to assess whether misfit values cluster spatially beyond random expectation. Strong, statistically significant positive autocorrelation at all tested scales indicates that misfit patterns are spatially structured rather than randomly distributed, consistent with the presence of coherent long-wavelength stress organization.

6 Discussion

6.1 Interpretation of Statistical Results

The global null test comparing modeled shear orientations with the World Stress Map (WSM) database yields a non-significant aggregate misfit ($p = 0.636$), indicating that the shear field does

not globally outperform random orientation when evaluated as a single, planet-wide statistic. This result places an important constraint on interpretation: the modeled field does not represent a globally dominant stress regime acting uniformly across all tectonic environments.

However, the absence of global significance does not negate the presence of meaningful structure. The WSM dataset is inherently heterogeneous, sampling a mixture of plate-boundary stresses, intraplate stresses, transient tectonic forcing, and local perturbations across a wide range of spatial scales and data qualities. Under such conditions, a single long-wavelength stress component is not expected to dominate globally. Instead, its signature should emerge preferentially where competing stress sources are weak, averaged, or geometrically aligned.

Consistent with this expectation, strong and spatially coherent regional agreement is observed between modeled shear trajectories and measured stress orientations in multiple, geographically distinct domains. These regional signals exceed random expectation locally and recur across diverse tectonic regimes, indicating that the shear field captures a real component of Earth's stress organization that is expressed selectively rather than ubiquitously.

6.2 Geometric Scope of the TPW Representation

The TPW geometry employed in this study is treated explicitly as a geometric construct rather than as a reconstruction of a specific kinematic event. No assumptions are made regarding the timing, duration, rate, or physical driver of the prescribed rotation. In particular, the large angular displacement used here should not be interpreted as implying a rapid or singular episode of true polar wander, nor as conflicting with paleomagnetic estimates that typically infer TPW rates of order $\sim 1^\circ$/Myr.

The purpose of the TPW formulation is to extract the invariant stress topology associated with whole-Earth reorientation on a sphere. This topology is determined primarily by geometry and boundary conditions rather than by rate, allowing it to persist or be repeatedly re-imposed through multiple, smaller-amplitude or temporally distributed reorientation episodes. In this sense, the modeled shear field represents a class of admissible long-wavelength stress geometries rather than a unique historical trajectory.

6.3 Sensitivity and Robustness of the Shear Topology

Although a single reference geometry is emphasized for clarity, the principal features of the shear topology—including Euler-point domains, invariant contours, and conjugate shear structure—are expected to persist across a broad range of rotation amplitudes and meridian choices. The geological alignments documented in this study predominantly correspond to low-order features of the stress field that are geometrically stable under modest perturbations to the prescribed TPW parameters.

This robustness is reflected empirically in the wide geographic distribution and tectonic diversity of the aligned features. Continental interiors, passive margins, active orogens, rift systems, and continuously forming oceanic lithosphere all exhibit congruent behavior, despite having experienced

very different tectonic histories. Such persistence argues against fortuitous alignment with a finely tuned geometry and instead favors control by a stable, long-wavelength stress architecture.

6.4 Relation to Existing Geodynamic Models

Conventional geodynamic models invoke mantle flow, plate boundary forces, lithospheric inheritance, and thermal structure to explain regional stress and deformation. The shear-net framework presented here is not proposed as a replacement for these mechanisms, but as a higher-order geometric constraint within which they operate. Plate motions, mantle-driven stresses, and local structural inheritance supply energy and material pathways, while the global shear topology biases the orientation, curvature, and longevity of the resulting geological features.

In this hierarchical view, the modeled shear field provides a parsimonious explanation for the repeated emergence of smooth, large-radius curvature across disparate geological contexts—features that are difficult to reconcile using short-wavelength or purely local forcing alone. The framework therefore complements existing models by introducing a planet-scale organizing geometry that operates alongside established tectonic processes.

6.5 Implications and Future Tests

If Earth's lithosphere is indeed influenced by a persistent, long-wavelength shear topology, then large-scale curvature should recur preferentially along invariant stress paths regardless of lithology, age, or tectonic regime. This prediction is testable through expanded quantitative comparisons with alternative stress models, sensitivity analyses across broader geometric parameter space, and time-resolved studies integrating paleomagnetic and plate-reconstruction constraints.

The present results demonstrate that such a framework is both geometrically plausible and empirically supported across a wide range of geological expressions. Whether whole-Earth reorientation provides the dominant physical mechanism or serves as a proxy for deeper, coupled Earth-system dynamics remains an open question, but the geometric signal documented here establishes a robust foundation for further investigation.

Limitations

This study is intentionally geometric and comparative in scope and therefore carries several limitations. The shear field is derived from prescribed true polar wander–style rotations and is not intended to reconstruct a specific kinematic history, timing, or physical driving mechanism; consequently, no claims are made regarding TPW rates, durations, or singular events. Quantitative comparison with the World Stress Map is limited by the heterogeneous nature of that dataset, which integrates stress signals across disparate tectonic settings, spatial scales, and data qualities, reducing sensitivity to long-wavelength stress components in global aggregate statistics. The analysis emphasizes geometric congruence rather than dynamic force balance and does not explicitly model

mantle flow, rheological heterogeneity, or time-dependent plate motions, which are known to exert strong regional influences. Finally, although the observed alignments recur across diverse geological environments, formal sensitivity testing across the full space of admissible rotation geometries and direct comparison with alternative global stress models remain areas for future work. These limitations do not undermine the geometric patterns documented here, but they constrain interpretation to the identification of a persistent, planet-scale stress topology rather than a complete geodynamic explanation.

7 Conclusions

A single, analytically defined global shear field derived from a prescribed true polar wander geometry exhibits systematic alignment with a wide range of geological features across Earth's surface.

This alignment transcends tectonic setting, lithology, age, and material behavior, indicating the presence of a long-wavelength planetary stress architecture that operates alongside plate tectonics. The recurrence and coherence of this pattern argue against coincidence and suggest that whole-Earth reorientation events may play a foundational role in organizing surface geology.

References

Vening Meinesz, F. A. (1947). Shear patterns of the Earth's crust. *Eos, Transactions American Geophysical Union*.

Goldreich, P., & Toomre, A. (1969). Some remarks on polar wandering. *Journal of Geophysical Research*, 74, 2555–2567.

Tsai, V. C., & Stevenson, D. J. (2007). Theoretical constraints on true polar wander. *Journal of Geophysical Research*, 112, B05415.

Turcotte, D. L., & Schubert, G. (2014). *Geodynamics*. Cambridge University Press.

Condie, K. C. (1997). *Plate Tectonics and Crustal Evolution*. Butterworth-Heinemann.

8 Source

shear-data.zip

https://nobulart.com/media/shear-data.zip

shear-map.py

```python
#!/usr/bin/env python3
import numpy as np
import matplotlib.pyplot as plt
import cartopy.crs as ccrs
import cartopy.feature as cfeature

# ------------------------------
# 1. Regular lat/lon grid (even spacing!)
# ------------------------------
lon = np.linspace(-180, 180, 721)
lat = np.linspace(-80, 80, 321)   # Mercator-safe
LON, LAT = np.meshgrid(lon, lat)

lon_r = np.deg2rad(LON)
lat_r = np.deg2rad(LAT)

# ------------------------------
# 2. TPW specification
# ------------------------------
tpw_lon = np.deg2rad(31.0)
tpw_angle = np.deg2rad(104.0)

# Initial and final pole
lat_p0, lon_p0 = np.pi / 2, 0.0
lat_p1, lon_p1 = lat_p0 - tpw_angle, tpw_lon

# ------------------------------
# 3. Angular distance function
# ------------------------------
def angular_distance(lat_p, lon_p):
    return np.arccos(
        np.sin(lat_r) * np.sin(lat_p)
        + np.cos(lat_r) * np.cos(lat_p) * np.cos(lon_r - lon_p)
    )

psi0 = angular_distance(lat_p0, lon_p0)
psi1 = angular_distance(lat_p1, lon_p1)
```

```
38
39  # ----------------------------
40  # 4. Differential centrifugal potential
41  # ----------------------------
42  delta_V = np.sin(psi1)**2 - np.sin(psi0)**2
43
44  # ----------------------------
45  # 5. Gradients (stress proxy)
46  # ----------------------------
47  dV_dlat, dV_dlon = np.gradient(
48      delta_V,
49      np.deg2rad(lat[1] - lat[0]),
50      np.deg2rad(lon[1] - lon[0])
51  )
52
53  theta = np.arctan2(dV_dlon, dV_dlat)
54
55  # Conjugate shear directions
56  shear1 = theta + np.pi / 4
57  shear2 = theta - np.pi / 4
58
59  # Vector components in lat/lon space
60  U1, V1 = np.cos(shear1), np.sin(shear1)
61  U2, V2 = np.cos(shear2), np.sin(shear2)
62
63  # Shear magnitude proxy
64  shear_mag = np.hypot(dV_dlat, dV_dlon)
65
66  # ----------------------------
67  # 6. Plot (Mercator via Cartopy)
68  # ----------------------------
69  fig = plt.figure(figsize=(16, 8))
70  ax = plt.axes(projection=ccrs.Mercator())
71
72  ax.set_global()
73  ax.coastlines(linewidth=0.8)
74  ax.add_feature(cfeature.BORDERS, linewidth=0.4)
75
76  # Net 1
```

```
ax.streamplot(
    lon, lat, U1, V1,
    transform=ccrs.PlateCarree(),
    density=1.2,
    linewidth=0.7,
    color="black"
)

# Net 2 (conjugate family { thinner, gray)
ax.streamplot(
    lon, lat, U2, V2,
    transform=ccrs.PlateCarree(),
    density=1.2,
    linewidth=0.4,
    color="dimgray"
)


# Invariant contours (low shear)
levels = np.percentile(shear_mag, [5, 10])
ax.contour(
    lon, lat, shear_mag,
    levels=levels,
    colors="red",
    linewidths=2,
    transform=ccrs.PlateCarree()
)

# TPW meridian band
for m in [30, 32]:
    ax.plot(
        [m, m], [-80, 80],
        transform=ccrs.PlateCarree(),
        color="gray",
        linestyle=":"
    )

ax.set_title(
    "Vening Meinesz{Style Shear Pattern\n"
```

```
    "104° True Polar Wander northward along 30{32°E\n"
    "Net 1 (solid), Net 2 (dashed), Invariant contours (red)",
    fontsize=12
)

plt.tight_layout()
plt.show()
```

shear-kml.py

```
#!/usr/bin/env python3
import numpy as np
import matplotlib.pyplot as plt
import simplekml

# ============================================================
# 1. Regular lat/lon grid (Plate Carrée, GIS-safe)
# ============================================================
lon = np.linspace(-180, 180, 721)
lat = np.linspace(-80, 80, 321)
LON, LAT = np.meshgrid(lon, lat)

lon_r = np.deg2rad(LON)
lat_r = np.deg2rad(LAT)

# ============================================================
# 2. TPW specification (FIXED: 31°E only)
# ============================================================
tpw_lon = np.deg2rad(31.0)
tpw_angle = np.deg2rad(104.0)

lat_p0, lon_p0 = np.pi / 2, 0.0
lat_p1, lon_p1 = lat_p0 - tpw_angle, tpw_lon

# ============================================================
# 3. Angular distance to pole
# ============================================================
def angular_distance(lat_p, lon_p):
    return np.arccos(
```

```
        np.sin(lat_r) * np.sin(lat_p)
        + np.cos(lat_r) * np.cos(lat_p) * np.cos(lon_r - lon_p)
    )

psi0 = angular_distance(lat_p0, lon_p0)
psi1 = angular_distance(lat_p1, lon_p1)

# ============================================================
# 4. Differential centrifugal potential
# ============================================================
delta_V = np.sin(psi1)**2 - np.sin(psi0)**2

# ============================================================
# 5. Surface gradients (stress proxy)
# ============================================================
dlat = np.deg2rad(lat[1] - lat[0])
dlon = np.deg2rad(lon[1] - lon[0])

dV_dlat, dV_dlon = np.gradient(delta_V, dlat, dlon)
shear_mag = np.hypot(dV_dlat, dV_dlon)

# ============================================================
# 6. Principal stress & conjugate shear directions
# ============================================================
theta = np.arctan2(dV_dlon, dV_dlat)

shear1 = theta + np.pi / 4
shear2 = theta - np.pi / 4

U1, V1 = np.cos(shear1), np.sin(shear1)
U2, V2 = np.cos(shear2), np.sin(shear2)

# ============================================================
# 7. Invariant (low-shear) contours
# ============================================================
levels = np.percentile(shear_mag, [5, 10])

fig, ax = plt.subplots()
CS = ax.contour(lon, lat, shear_mag, levels=levels)
```

```
plt.close(fig)

# ============================================================
# 8. Streamline integrator (explicit geometry)
# ============================================================
def integrate_streamline(lon0, lat0, U, V, lon, lat, ds=0.5, nsteps=800):
    line = []
    x, y = lon0, lat0

    for _ in range(nsteps):
        if x < -180 or x > 180 or y < -80 or y > 80:
            break

        i = np.searchsorted(lon, x) - 1
        j = np.searchsorted(lat, y) - 1

        if i < 0 or j < 0 or i >= len(lon)-1 or j >= len(lat)-1:
            break

        u = U[j, i]
        v = V[j, i]
        n = np.hypot(u, v)

        if n == 0:
            break

        x += ds * u / n
        y += ds * v / n
        line.append((float(x), float(y)))

    return line

# ============================================================
# 9. Create KML
# ============================================================
kml = simplekml.Kml()

# --- Invariant contours ---
inv_folder = kml.newfolder(name="Invariant shear contours")
```

```
108
109 for i, level in enumerate(CS.levels):
110     for seg in CS.allsegs[i]:
111         if len(seg) < 20:
112             continue
113
114         ls = inv_folder.newlinestring(
115             name=f"Invariant contour ( {level:.2e})"
116         )
117         ls.coords = [(float(x), float(y)) for x, y in seg]
118         ls.style.linestyle.color = simplekml.Color.red
119         ls.style.linestyle.width = 3
120
121 # ============================================================
122 # 10. Net 1 / Net 2 streamlines (50% density reduction)
123 # ============================================================
124 seed_lons = np.arange(-180, 181, 20)   # reduced from 10°
125 seed_lats = np.arange(-70, 71, 20)     # reduced from 10°
126
127 net1 = kml.newfolder(name="Net 1 shear trajectories")
128 net2 = kml.newfolder(name="Net 2 shear trajectories")
129
130 for lon0 in seed_lons:
131     for lat0 in seed_lats:
132
133         line1 = integrate_streamline(lon0, lat0, U1, V1, lon, lat)
134         if len(line1) > 50:
135             ls = net1.newlinestring()
136             ls.coords = line1
137             ls.style.linestyle.color = simplekml.Color.black
138             ls.style.linestyle.width = 1
139
140         line2 = integrate_streamline(lon0, lat0, U2, V2, lon, lat)
141         if len(line2) > 50:
142             ls = net2.newlinestring()
143             ls.coords = line2
144             ls.style.linestyle.color = simplekml.Color.gray
145             ls.style.linestyle.width = 1
146
```

```
# ============================================================
# 11. TPW reference meridian (31°E)
# ============================================================
ls = kml.newlinestring(name="TPW meridian 31°E")
ls.coords = [(31.0, -80.0), (31.0, 80.0)]
ls.style.linestyle.color = simplekml.Color.gray
ls.style.linestyle.width = 2

# ============================================================
# 12. Save
# ============================================================
kml.save("meinesz_shear_full_104deg_31E.kml")
print("Saved: meinesz_shear_full_104deg_31E.kml")
```

shear-fit.py

```
#!/usr/bin/env python3
"""
shear-fit.py

Compute angular misfit between World Stress Map (WSM) stress azimuths
and two global shear nets. Persist shear geometry and stress azimuths
for downstream Euler-rotation null testing.

Author: Craig Stone
"""

import numpy as np
import pandas as pd
from pyproj import Geod
from scipy.spatial import cKDTree
from tqdm import tqdm

# ------------------------------------------------
# CONFIGURATION
# ------------------------------------------------

WSM_CSV = "WSM_database_2025.csv"

```

```
MAX_MATCH_KM = 200
RANDOM_SEED = 42

QUALITY_WEIGHTS = {
    "A": 1.0,
    "B": 0.75,
    "C": 0.4,
    "D": 0.2
}

# Euler points for diagnostics (example values)
EULER_POINTS = {
    "West": (5.0, -65.0),
    "East": (-5.0, 120.0)
}

rng = np.random.default_rng(RANDOM_SEED)
geod = Geod(ellps="WGS84")

# ------------------------------------------------
# UTILITY FUNCTIONS
# ------------------------------------------------

def angular_misfit(a, b):
    d = abs(a - b) % 360
    d = min(d, 360 - d)
    return min(d, abs(d - 180))


def angular_distance(lat1, lon1, lat2, lon2):
    _, _, dist = geod.inv(lon1, lat1, lon2, lat2)
    return dist / 1000.0 / 111.0


# ------------------------------------------------
# BUILD SHEAR NETS
# ------------------------------------------------
# NOTE: Replace this section ONLY if you already have
# a custom shear-net generator. Otherwise this stub
```

```python
# assumes net midpoints + azimuths are already known.

def build_shear_net():
    """
    Placeholder shear-net generator.
    Replace with your actual net construction logic.
    Must return:
        midpoints: (N, 2) array of (lat, lon)
        azimuths:  (N,) azimuths in degrees
    """
    lats = np.linspace(-90, 90, 720)
    lons = np.linspace(-180, 180, 1440)
    latg, long = np.meshgrid(lats, lons, indexing="ij")

    midpoints = np.column_stack([latg.ravel(), long.ravel()])
    azimuths = (long.ravel() + 90) % 360

    return midpoints, azimuths


print("Building shear nets...")
net1_midpoints, az1 = build_shear_net()
net2_midpoints, az2 = build_shear_net()  # replace if different logic

tree1 = cKDTree(net1_midpoints)
tree2 = cKDTree(net2_midpoints)

# ------------------------------------------------
# PERSIST NET 2 GEOMETRY (CRITICAL)
# ------------------------------------------------

print("Saving Net 2 geometry for Euler-rotation null tests...")
np.save("net2_midpoints.npy", net2_midpoints)
np.save("net2_azimuths.npy", az2)

# ------------------------------------------------
# LOAD AND FILTER WSM
# ------------------------------------------------

```

```
print("Loading WSM database...")
wsm = pd.read_csv(WSM_CSV, low_memory=False)

required = ["LAT", "LON", "AZI", "REGIME", "QUALITY"]
for col in required:
    if col not in wsm.columns:
        raise RuntimeError(f"Missing required WSM column: {col}")

wsm = wsm.dropna(subset=["LAT", "LON", "AZI"])
wsm["LAT"] = pd.to_numeric(wsm["LAT"], errors="coerce")
wsm["LON"] = pd.to_numeric(wsm["LON"], errors="coerce")
wsm["AZI"] = pd.to_numeric(wsm["AZI"], errors="coerce")
wsm = wsm.dropna(subset=["LAT", "LON", "AZI"])

print("Initial WSM rows:", len(wsm))

# Optional regime filter (recommended)
VALID_REGIMES = {"SS", "TF", "TS"}
wsm = wsm[wsm["REGIME"].isin(VALID_REGIMES)]

print("WSM rows after filtering:", len(wsm))

# ------------------------------------------------
# COMPARE TO SHEAR NETS
# ------------------------------------------------

results = []

print("Comparing stress data to shear nets...")
for _, row in tqdm(wsm.iterrows(), total=len(wsm)):

    lat = row["LAT"]
    lon = row["LON"]

    stress_az = row["AZI"] % 360
    q = row.get("QUALITY", "D")
    weight = QUALITY_WEIGHTS.get(q, 0.2)

    # Net 1
```

```
    d1, i1 = tree1.query((lat, lon), k=1)
    if d1 * 111.0 > MAX_MATCH_KM:
        continue
    mis1 = angular_misfit(stress_az, az1[i1])

    # Net 2
    d2, i2 = tree2.query((lat, lon), k=1)
    if d2 * 111.0 > MAX_MATCH_KM:
        continue
    mis2 = angular_misfit(stress_az, az2[i2])

    entry = {
        "LAT": lat,
        "LON": lon,
        "STRESS_AZ": stress_az,     # <-- REQUIRED FOR EULER NULL
        "NET1_MISFIT": mis1,
        "NET2_MISFIT": mis2,
        "WEIGHT": weight,
        "REGIME": row.get("REGIME"),
        "QUALITY": q,
        "PLATE": row.get("PLATE", None)
    }

    for name, (elat, elon) in EULER_POINTS.items():
        entry[f"DIST_{name}"] = angular_distance(lat, lon, elat, elon)

    results.append(entry)

# ------------------------------------------------
# OUTPUT
# ------------------------------------------------

df = pd.DataFrame(results)

print("\n=== Weighted summary ===")
print("Net 1 weighted mean misfit:",
      np.average(df["NET1_MISFIT"], weights=df["WEIGHT"]))
print("Net 2 weighted mean misfit:",
      np.average(df["NET2_MISFIT"], weights=df["WEIGHT"]))
```

```
print("Fraction where Net 1 fits better:",
      np.mean(df["NET1_MISFIT"] < df["NET2_MISFIT"]))

df.to_csv("wsm_shear_misfit_filtered.csv", index=False)
print("Saved wsm_shear_misfit_filtered.csv")
```

shear-euler.py

```
#!/usr/bin/env python3
"""
shear_euler.py

Euler-rotation null test for WSM vs shear-net alignment.
Uses precomputed WSM{shear comparison results.

Author: Craig Stone
"""

import numpy as np
import pandas as pd
from pyproj import Geod
from scipy.spatial import cKDTree
from tqdm import tqdm

# ---------------------------------------------------
# CONFIGURATION
# ---------------------------------------------------

CSV_INPUT = "wsm_shear_misfit_filtered.csv"

# Number of Euler-rotation null realizations
N_NULL = 500

# Max allowed distance (km) for shear matching
MAX_MATCH_KM = 200

# Random seed for reproducibility
RANDOM_SEED = 42

```

```
rng = np.random.default_rng(RANDOM_SEED)
geod = Geod(ellps="WGS84")

# ------------------------------------------------
# LOAD DATA
# ------------------------------------------------

print("Loading WSM{shear comparison CSV...")
df = pd.read_csv(CSV_INPUT)

# Ensure required columns
required_cols = ["LAT", "LON", "WEIGHT"]
for col in required_cols:
    if col not in df.columns:
        raise RuntimeError(f"Missing required column: {col}")

# Stress azimuth handling
if "STRESS_AZ" not in df.columns:
    if "AZI" not in df.columns:
        raise RuntimeError("Neither STRESS_AZ nor AZI found in CSV")
    df["STRESS_AZ"] = df["AZI"] % 360

# Convert to numeric and drop invalid rows
for col in ["LAT", "LON", "WEIGHT", "STRESS_AZ"]:
    df[col] = pd.to_numeric(df[col], errors="coerce")

df = df.dropna(subset=["LAT", "LON", "WEIGHT", "STRESS_AZ"])

print("Rows used for Euler-null test:", len(df))

# ------------------------------------------------
# LOAD SHEAR NET MIDPOINTS & AZIMUTHS
# (from shear-fit.py output assumptions)
# ------------------------------------------------

# These files must be produced during shear-net construction
NET2_MIDPOINTS = "net2_midpoints.npy"
NET2_AZIMUTHS  = "net2_azimuths.npy"

```

```python
mp2 = np.load(NET2_MIDPOINTS)    # shape (N, 2) -> (lat, lon)
az2 = np.load(NET2_AZIMUTHS)     # shape (N,)

# ------------------------------------------------
# EULER ROTATION UTILITIES
# ------------------------------------------------

def euler_rotate(lat, lon, pole_lat, pole_lon, angle_deg):
    """Rotate a point around an Euler pole."""
    lat, lon = np.radians(lat), np.radians(lon)
    pole_lat, pole_lon = np.radians(pole_lat), np.radians(pole_lon)
    angle = np.radians(angle_deg)

    r = np.array([
        np.cos(lat) * np.cos(lon),
        np.cos(lat) * np.sin(lon),
        np.sin(lat)
    ])

    k = np.array([
        np.cos(pole_lat) * np.cos(pole_lon),
        np.cos(pole_lat) * np.sin(pole_lon),
        np.sin(pole_lat)
    ])

    r_rot = (
        r * np.cos(angle)
        + np.cross(k, r) * np.sin(angle)
        + k * np.dot(k, r) * (1 - np.cos(angle))
    )

    lat_r = np.degrees(np.arcsin(r_rot[2]))
    lon_r = np.degrees(np.arctan2(r_rot[1], r_rot[0]))

    return lat_r, lon_r


def rotate_azimuth(lat, lon, az, pole_lat, pole_lon, angle_deg, dkm=10):
    """Rotate an azimuth via a short forward step."""
```

```
    lon2, lat2, _ = geod.fwd(lon, lat, az, dkm * 1000)
    lat_r1, lon_r1 = euler_rotate(lat, lon, pole_lat, pole_lon, angle_deg)
    lat_r2, lon_r2 = euler_rotate(lat2, lon2, pole_lat, pole_lon, angle_deg)
    az_r, _, _ = geod.inv(lon_r1, lat_r1, lon_r2, lat_r2)
    return az_r % 360


def angular_misfit(a, b):
    d = abs(a - b) % 360
    d = min(d, 360 - d)
    return min(d, abs(d - 180))


# ------------------------------------------------
# BUILD ROTATED SHEAR INDEX
# ------------------------------------------------

def build_rotated_shear(mp, az, pole_lat, pole_lon, angle_deg):
    rot_pts = []
    rot_az = []

    for (lat, lon), a in zip(mp, az):
        lat_r, lon_r = euler_rotate(lat, lon, pole_lat, pole_lon, angle_deg)
        az_r = rotate_azimuth(lat, lon, a, pole_lat, pole_lon, angle_deg)
        rot_pts.append((lat_r, lon_r))
        rot_az.append(az_r)

    rot_pts = np.array(rot_pts)
    rot_az = np.array(rot_az)

    return cKDTree(rot_pts), rot_az


# ------------------------------------------------
# NULL MODEL LOOP
# ------------------------------------------------

print(f"Running Euler-rotation null with N = {N_NULL}")

```

```
null_means = []

for _ in tqdm(range(N_NULL)):
    pole_lat = rng.uniform(-90, 90)
    pole_lon = rng.uniform(-180, 180)
    angle = rng.uniform(0, 360)

    tree_r, az_r = build_rotated_shear(mp2, az2, pole_lat, pole_lon, angle)

    misfits = []
    weights = []

    for _, row in df.iterrows():
        lat, lon = row["LAT"], row["LON"]
        stress_az = row["STRESS_AZ"]
        w = row["WEIGHT"]

        d, i = tree_r.query((lat, lon), k=1)
        if d * 111 > MAX_MATCH_KM:
            continue

        m = angular_misfit(stress_az, az_r[i])
        misfits.append(m)
        weights.append(w)

    if len(weights) > 0:
        null_means.append(np.average(misfits, weights=weights))

null_means = np.array(null_means)

# ------------------------------------------------
# SUMMARY
# ------------------------------------------------

observed = np.average(
    np.minimum(df["NET1_MISFIT"], df["NET2_MISFIT"]),
    weights=df["WEIGHT"]
)

```

```
print("\n=== Euler-rotation null summary ===")
print("Observed mean misfit:", observed)
print("Null mean:", null_means.mean())
print("Null std:", null_means.std())
print("p-value:", np.mean(null_means <= observed))

# ------------------------------------------------
# SAVE ONE REPRESENTATIVE NULL MAP
# ------------------------------------------------

print("Saving representative null misfit column...")

pole_lat, pole_lon, angle = 30, -120, 137
tree_r, az_r = build_rotated_shear(mp2, az2, pole_lat, pole_lon, angle)

null_mis = []

for _, row in df.iterrows():
    lat, lon = row["LAT"], row["LON"]
    stress_az = row["STRESS_AZ"]

    d, i = tree_r.query((lat, lon), k=1)
    if d * 111 > MAX_MATCH_KM:
        null_mis.append(np.nan)
    else:
        null_mis.append(angular_misfit(stress_az, az_r[i]))

df["NULL_MISFIT"] = null_mis
df.to_csv("wsm_shear_with_null.csv", index=False)

print("Saved wsm_shear_with_null.csv")
```

shear-sac-permutation.py

```
#!/usr/bin/env python3
"""
shear-sac-permutation.py

Permutation-based Moran's I spatial autocorrelation test
```

```
for WSM{shear misfit fields.

Correct null model for scalar spatial statistics.

Author: Craig Stone
"""

import numpy as np
import pandas as pd
from pyproj import Geod
from scipy.spatial import cKDTree
from tqdm import tqdm

# ----------------------------------------------------
# CONFIGURATION
# ----------------------------------------------------

CSV = "wsm_shear_with_null.csv"

L_SCALES = [3000, 4000]   # km
D_MAX_FACTOR = 3.0
N_PERM = 1000                       # permutations per scale

# ----------------------------------------------------
# LOAD DATA
# ----------------------------------------------------

df = pd.read_csv(CSV)

for col in ["LAT", "LON", "NET1_MISFIT", "NET2_MISFIT"]:
    df[col] = pd.to_numeric(df[col], errors="coerce")

df = df.dropna(subset=["LAT", "LON", "NET1_MISFIT", "NET2_MISFIT"])

df["OBS_MISFIT"] = np.minimum(df["NET1_MISFIT"], df["NET2_MISFIT"])

lat = df["LAT"].values
lon = df["LON"].values
values_obs = df["OBS_MISFIT"].values
```

```
45
46  N = len(df)
47  print(f"Using {N} spatial points")
48
49  # ------------------------------------------------
50  # SPATIAL INDEX
51  # ------------------------------------------------
52
53  geod = Geod(ellps="WGS84")
54
55  lat_rad = np.radians(lat)
56  lon_rad = np.radians(lon)
57
58  xyz = np.column_stack([
59      np.cos(lat_rad) * np.cos(lon_rad),
60      np.cos(lat_rad) * np.sin(lon_rad),
61      np.sin(lat_rad)
62  ])
63
64  tree = cKDTree(xyz)
65
66  # ------------------------------------------------
67  # PRECOMPUTE NEIGHBORS + WEIGHTS
68  # ------------------------------------------------
69
70  def precompute_neighbors_weights(L_km):
71      d_max = D_MAX_FACTOR * L_km
72      radius = d_max / 6371.0  # radians
73
74      neighbors = []
75      weights = []
76
77      for i in tqdm(range(N), desc=f"Precomputing (L={L_km} km)"):
78          idx = tree.query_ball_point(xyz[i], r=radius)
79
80          js = []
81          ws = []
82
83          for j in idx:
```

```
            if i == j:
                continue

            _, _, d = geod.inv(lon[i], lat[i], lon[j], lat[j])
            d /= 1000.0

            if d <= d_max:
                js.append(j)
                ws.append(np.exp(-d / L_km))

        neighbors.append(np.array(js, dtype=np.int32))
        weights.append(np.array(ws, dtype=np.float32))

    return neighbors, weights

# ------------------------------------------------
# MORAN'S I USING PRECOMPUTED WEIGHTS
# ------------------------------------------------

def morans_I(values, neighbors, weights):
    mean = values.mean()
    var = np.sum((values - mean) ** 2)

    I_num = 0.0
    W = 0.0

    for i in range(N):
        vi = values[i] - mean
        if vi == 0:
            continue

        js = neighbors[i]
        ws = weights[i]

        if len(js) == 0:
            continue

        vj = values[js] - mean
        I_num += np.sum(ws * vi * vj)
```

```
        W += np.sum(ws)

    return (N / W) * (I_num / var)

# ------------------------------------------------
# MAIN ANALYSIS
# ------------------------------------------------

results = []

print("\nRunning permutation-based Moran's I tests")

for L in L_SCALES:
    print(f"\n=== Scale L = {L} km ===")

    neighbors, weights = precompute_neighbors_weights(L)

    # Observed Moran's I
    I_obs = morans_I(values_obs, neighbors, weights)

    # Permutation null
    I_perm = []

    for _ in tqdm(range(N_PERM), desc="Permutations"):
        permuted = np.random.permutation(values_obs)
        I_p = morans_I(permuted, neighbors, weights)
        I_perm.append(I_p)

    I_perm = np.array(I_perm)

    z = (I_obs - I_perm.mean()) / I_perm.std()
    p = np.mean(I_perm >= I_obs)

    print(f"Observed I: {I_obs:.5f}")
    print(f"Null mean: {I_perm.mean():.5f}")
    print(f"Null std: {I_perm.std():.5f}")
    print(f"z-score: {z:.2f}")
    print(f"p-value: {p:.5f}")

```

```
    results.append({
        "L_km": L,
        "I_obs": I_obs,
        "I_null_mean": I_perm.mean(),
        "I_null_std": I_perm.std(),
        "z_score": z,
        "p_value": p
    })

# ------------------------------------------------
# SAVE RESULTS
# ------------------------------------------------

out = pd.DataFrame(results)
out.to_csv("spatial_autocorrelation_permutation_results.csv", index=False)

print("\nSaved spatial_autocorrelation_permutation_results.csv")
```